GFZ
Helmholtz Centre
POTSDAM

GeoMod2014

Modelling in Geosciences

Programme & Extended Abstracts

31 August - 5 September 2014

Editors:
Kirsten Elger
Øystein Thordén Haug
Malte Ritter

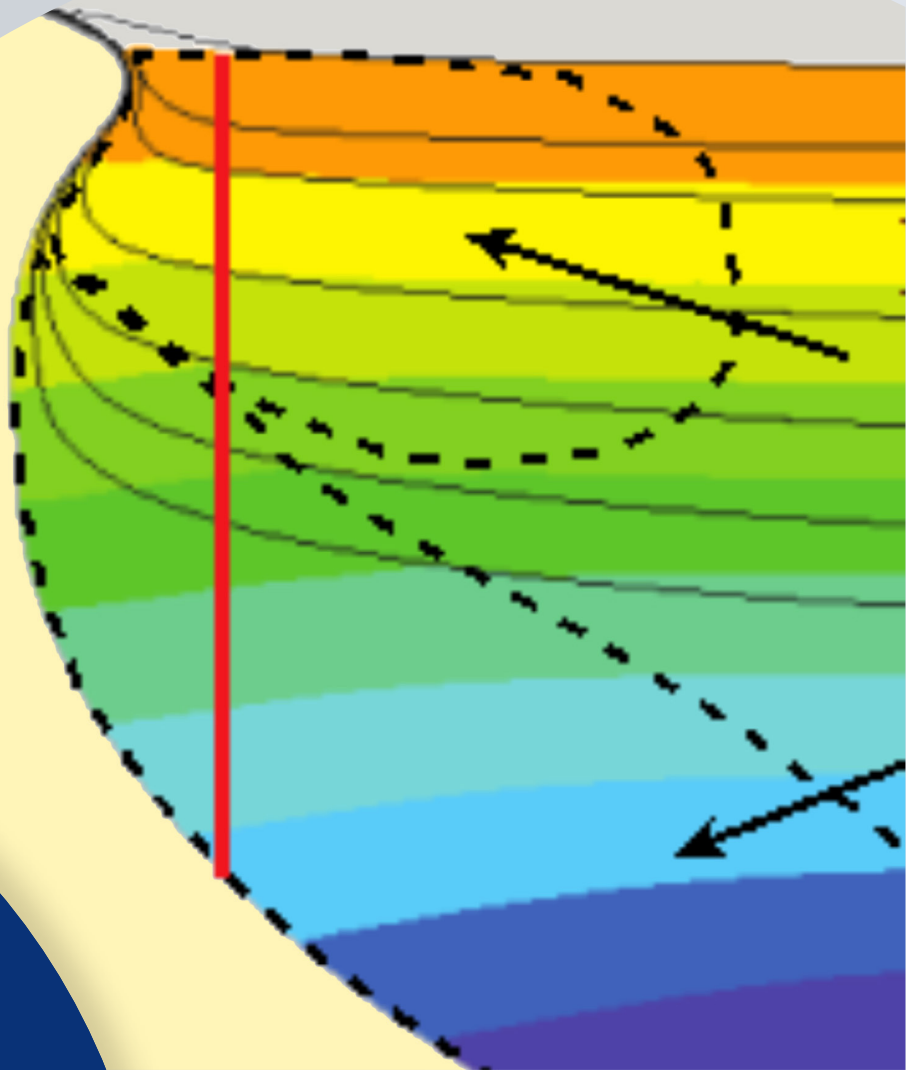

Session V
Rheology

Conveners:
Georg Dresen (GFZ/U Potsdam)
Hiroki Sone (GFZ)

DFG GeoX GeoSim

Recommended Citation

Elger, K; Haug, Ø. T.; Ritter, M. C. (Eds), (2014): Proceedings of GeoMod2014 – Modelling in Geosciences: Programme and Extended Abstracts 31 August–5 September 2014, GeoMod2014 – Modelling in Geosciences (Potsdam 2014), Potsdam: GFZ German Research Centre for Geosciences. DOI: http://doi.org/10.2312/GFZ.geomod.2014.001.

Disclaimer and Copyright

Imprint

Publisher
Helmholtz Centre Potsdam
GFZ German Research Centre for Geosciences
Telegrafenberg
14473 Potsdam
Published in Potsdam, Germany

Editors
Kirsten Elger
Øystein T. Haug
Malte C. Ritter

doi: 10.2312/GFZ.geomod.2014.001

About this book

This volume contains the extended abstracts of contributions presented during GeoMod 2014 at the Helmholtz Centre Potsdam GFZ German Research Centre for Geosciences (GFZ Potsdam), showing the state of the art of the tectonic modeling community.

GeoMod is a biennial conference dedicated to latest results of analogue and numerical modelling of lithospheric and mantle deformation. It started in 2002 in Milan as RealMod2002, then moved to Lucerne (GeoMod2004), Florence (2008), Lisbon (2010), and Lausanne (2012).

GeoMod2014 took place from 31 August to 3 September 2014 with 138 participants from 25 countries on all continents. The scientific programme of GeoMod2014 was organized in seven topical sessions listed below. The conference was followed by a 2-day short course on "Constitutive Laws: from Observation to Implementation in Models" (including lectures, lab visits, and practical exercises), as well as a 1-day hands-on tutorial on the ASPECT numerical modelling software.

GeoMod2014 focused on rheology and deformation at a wide range of temporal and spatial scales: from earthquakes to long-term deformation, from microstructures to orogens and subduction systems. For the first time, the discipline of volcanotectonics was included, while the (mantle) geodynamics community was more strongly represented than in previous editions. The bridge to field geology has traditionally been strong. At GeoMod 2014, fitting to the focus on rheology, the rock mechanics community was also represented. We thank our sponsors DFG, GFZ Potsdam and Geo.X, the conveners and all participants for contributing to a successful conference.

The GeoMod2014 Committee

The Scientific Committee
Onno Oncken
Georg Dresen
Stephan Sobolev
Matthias Rosenau
Karen Leever

The Organising Committee
Kirsten Elger
Franziska Alberg
Students support: Zahra Amirzada, Felix Eckelmann, Øystein Thordén Haug, Shaoyang Li, Malte Ritter, Tasca Santimano, Sarah Schröder, Johannes Wagner

Sessions, Conveners, and keynote speakers

(Seismo-)tectonics
Conveners: Boris Kaus (U Mainz), Onno Oncken (GFZ/FU Berlin),
Keynotes: Kelin Wang (Geological Survey Canada, Alberta), Bertrand Maillot (U Cergy-Pontoise)

Tectonics & Surface Processes
Conveners: Fabien Graveleau (U Lille), Niels Hovius (GFZ/U Potsdam),
Keynotes: Ritske Huismans (U Bergen), Stéphane Dominguez (U Montpellier II)

Volcanism and Volcanotectonics
Conveners: Olivier Galland (U Oslo), Eoghan Holohan (GFZ)
Keynotes: Rikke Pedersen (U Iceland), Olivier Roche (U BP Clermont-Ferrand)

Geodynamics
Conveners: Francesca Funiciello (U Roma Tre), Stephan Sobolev (GFZ),
Keynotes: Anne Davaille (U Paris-Sud), Bernhard Steinberger (GFZ)

Rheology
Conveners: Georg Dresen (GFZ/U Potsdam), Hiroki Sone (GFZ),
Keynotes: Yuri Fialko (U California), Laurent Montési (U Maryland)

Fluids and Deformation
Conveners: Stephen Miller (U Bonn), Marcos Moreno Switt (GFZ),
Keynotes: Boris Galvan (U Bonn), Takeshi Tsuji (U Kyushu)

Methods and Materials (poster-only session)
Conveners: Matthias Rosenau (GFZ), Marcel Frehner (ETH Zürich)

Short course on "Constitutive Laws: from Observation to Implementation in Models"
Lecturers: Onno Oncken (GFZ Potsdam), Matthias Rosenau (GFZ Potsdam), Fabio Corbi (GFZ Potsdam), Georg Dresen (GFZ Potsdam), Stephan Sobolev (GFZ Potsdam), Sascha Brune (U Sydney)

Hands-on tutorial on "ASPECT: a next-generation geodynamic modelling software"
(Advanced Solver for Problems in Earth's ConvecTion)
Lecturers: Anne Glerum (Utrecht University), Juliane Dannberg (GFZ Potsdam). Supervised by Wolfgang Bangerth (Texas A&M University, ASPECT main developer), Stephan Sobolev (GFZ Potsdam), Bernhard Steinberger (GFZ Potsdam).

Contents

Session V.

Rheology

Session Description: Rheology

Conveners: Georg Dresen (GFZ/U Potsdam), Hiroki Sone (GFZ)

Rheology of the Lithosphere – What's new and where is this going? Localized and episodic deformation in the upper crust is intimately coupled to viscous flow of deeper layers of the upper lithosphere. The nature of this coupling in actively deforming regions such as mountain belts and large plate-bounding fault zones is complex and involving a broad range of governing physical processes potentially varying in space and time. In this session we wish to address open questions related to the rheology of crustal and upper mantle rocks and in particular span a bridge between constraints provided by laboratory and field studies to numerical modelling approaches of ductile deformation processes over a range of spatial and temporal scales.

Fold Geometry Toolbox 2: A New Tool to Estimate Mechanical Parameters and Shortening from Fold Geometry

Marta Adamuszek[1], Marcin Dabrowski[1,2], Daniel W. Schmid[2]

[1]*Polish Geological Institute – National Research Institute, Lower Silesia Branch, Poland*
[2]*Physics of Geological Processes, University of Oslo, 0316 Oslo, Norway*
e-mail: *marta.adamuszek@pgi.gov.pl*
session: *Rheology*

Rheological properties of rocks, deformation condition, and amount of shortening significantly influence shape of buckle folds during deformation. Understanding the relation between these parameters and the fold shape gives a possibility to interpret natural fold structures and consequently gain an insight into rock deformation at the geological scale. Range of mathematical relationships has been derived from the mechanical theory of folding to estimate material parameters and amount of shortening from the fold shape. The use of these relationships requires determination of the fold geometrical parameters such as fold arclength, amplitude, wavelength and thickness. An accurate estimation of the geometrical parameters is essential for the correct fold shape analysis. The major challenge in the fold geometry study is rooted in curvature analysis, which is highly sensitive to the presence of noise. The noise corrupts the curvature analysis and thus affects identification of hinges and inflection points, which are the reference points necessary to determine all the fold shape parameters.

In order to promote the accurate fold shape analysis, we developed Fold Geometry Toolbox (FGT) (Adamuszek et al., 2011). The toolbox deals with noisy interfaces and automatically determines the four parameters for a generic fold shape. The parameters are further employed in estimation of shortening and material properties using: Biot (1961, 1965), Currie et al. (1962), Sherwin and Chapple (1968), Fletcher (1974, 1977), Fletcher and Sherwin (1978) and Schmalholz and Podladchikov (2001) methods. FGT is open source, written in MATLAB. It is easy to use and comes with a graphical user interface.

The new version of FGT includes significant new functionality aimed at improving the fold shape analysis and presentation of the final results in a form of exportable tables and figures. The new enhancements also involve implementation of new methods for estimating shortening and mechanical parameters based on e.g. stretching of the folded layer back to the planar orientation using analytical Large Amplitude Folding method (Adamuszek et al., 2013) and finite element method based tools. Further changes in the toolbox include a possibility to: a) make a correction for obliquity of the fold section, b) modify manually the position of hinges and inflection points on the fold interfaces, c) analyse a single fold interface, d) exclude part of the fold train from the final fold analysis, and e) apply different filtering on different fold interfaces.

One of the new key features in FGT is EduFold application. The application is desired to illustrate the fold evolution with progressing shortening for user defined initial geometrical and mechanical parameters and amount of shortening. The evolution of the fold shape and the fold shape parameters can be illustrated for each time step on diagrams (Figure 1). The folding process is simulated using finite element method based MIL-

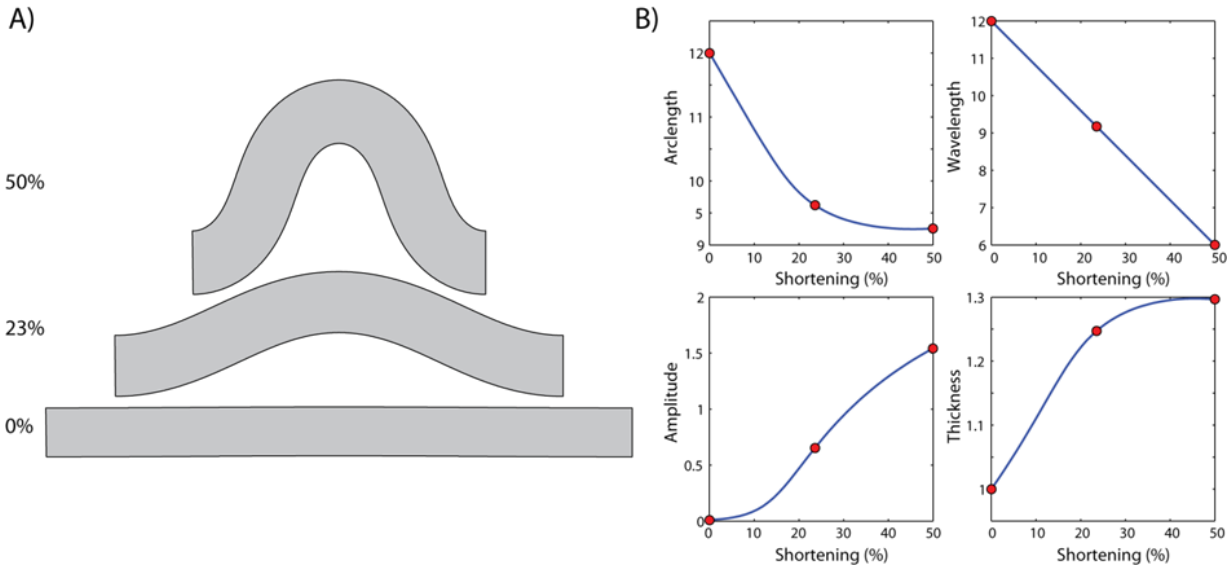

Fig. 1.: Results of the numerical simulation of fold evolution using EduFold application for initial amplitude A0=0.01, wavelength λ=12, thickness H=1, viscosity ratio R=100, and stress exponent n=1. A) Fold shape at shortening of 0%, 23%, and 50%. B) Evolution of fold geometry parameters as a function of shortening. Three points on the four diagrams refer to three shortening values 0%, 23%, and 50%.

AMIN solver (Dabrowski et al., 2008). The fold shape generated in the application can be further analysed in the toolbox. As a result, EduFold application has a great educational value. Geometrical analysis of the synthetically generated fold allows to investigate the relation between the input and output parameter values. This gives a user an opportunity to explore advantages and limitations of the mathematical relationships desired to analyse the fold shape.

References

Adamuszek M., Dabrowski M., Schmid D.W. 2011. Fold Geometry Toolbox - Automated determination of fold shape, shortening, and material properties Journal of Structural Geology, Vol. 33, p. 1406-1416

Adamuszek M., Schmid D.W., Dabrowski M., 2013, Theoretical analysis of large amplitude folding of a single viscous layer, Journal of Structural Geology, Vol. 48, p. 137–152

Biot, M.A., 1961. Theory of folding of stratified viscoelastic media and its implications in tectonics and orogenesis. Geological Society of America Bulletin 72 (11), 1595-1620.

Biot, M.A., 1965. Theory of similar folding of first and second kind. Geological Society of America Bulletin 76 (2), 251.

Currie, J.B., Patnode, H.W., Trump, R.P., 1962. Development of folds in sedimentary strata. Geological Society of America Bulletin 73, 655-674.

Dabrowski, M., Krotkiewski, M., Schmid, D.W., 2008. MILAMIN: MATLAB-based finite element method solver for large problems. Geochemistry Geophysics Geosystems 9.

Fletcher, R.C., 1974. Wavelength selection in folding of a single layer with power-law Rheology. American Journal of Science 274 (9), 1029-1043.

Fletcher, R.C., 1977. Folding of a single viscous layer: exact infinitesimal-amplitude solution. Tectonophysics 39, 593-606.

Fletcher, R.C., Sherwin, J.A., 1978. Arc lengths of single layer folds - Discussion of comparison

between Theory and Observation. American Journal of Science 278(8), 1085-1098.

Sherwin, J.A., Chapple, W.M., 1968. Wavelengths of single layer folds - a comparison between theory and observation. American Journal of Science 266 (3), 167-179.

Schmalholz, S.M., Podladchikov, Y.Y., 2001. Strain and competence contrast estimation from fold shape. Tectonophysics 340 (3-4), 195-213.

Mechanical anisotropy development and localization in two-phase composite rocks.

Marcin Dabrowski[1,2]

[1] *Computational Geology Laboratory, Polish Geological Institute - National Research Institute, Wroclaw, Poland*
[2] *Physics of Geological Processes, University of Oslo, Oslo, Norway*
e-mail: *mdabr@pgi.gov.pl*
session: *Rheology*

Introduction

An isotropic composite medium subject to viscous deformation develops compositional layering, which is initially parallel to the instantaneous stretching direction. The development of such structural anisotropy results in effectively anisotropic viscous properties, which favor layer-parallel shearing over layer-parallel stretching or shortening. Thus, to a first order approximation, monotonic hardening is expected in pure shear deformation. Non-coaxial deformation paths such as simple shear can lead to an initial hardening phase followed by overall weakening (Dabrowski et al, 2012). The behavior reflects a successive build-up of the shape and mechanical anisotropy concurrent with a progressive reorientation of the compositional layering into the shear direction. This results in a growing dominance of the weaker component (shear viscosity) over the stronger component (normal viscosity) of the effective anisotropic viscosity in determining the effective mechanical response of a composite rock in simple shear. The level and the rate of mechanical weakening available in two-phase composite systems consisting of weak inclusions depend chiefly on the inclusion fraction and the viscosity ratio. A varying inclusion fraction in a rock column subject to simple shear results in a non-homogeneous distribution of the shear rate. With strain-dependent weakening due to fabric development, which provides a positive-feedback mechanism, strain localization can occur. However, deforming anisotropic rocks may experience mechanical instabilities, e.g., internal boudinage or folding may develop during layer-parallel extension or shortening, respectively, resulting in both cases in a prominent overall weakening. In fact, the question that arises is as to whether viscous deformation of initially isotropic composite rocks can lead to a well-developed compositional layering before it is hampered by boudinage formation. With regard to the issue, the three critical questions are: (1) How does the rock fabric evolution depend on the mechanical properties of rock constituents, the inclusion fraction and the initial microstructure? (2) How does the mechanical (viscous) anisotropy relate to the overall shape anisotropy of a composite rock? (3) How does the internal boudinage development manifest in composite materials consisting of elongated inclusions rather than well-developed layers?

Methods

I will numerically investigate the development of shape preferred orientation and mechanical anisotropy in a composite two-phase rock undergoing stretching. A two-dimensional inclusion-host type of composite, in which an interconnected host embeds non-overlapping inclusions, is considered. Different inclusion fractions, shapes and size distributions are studied. The initial spatial distribution of the inclusions is intended to be

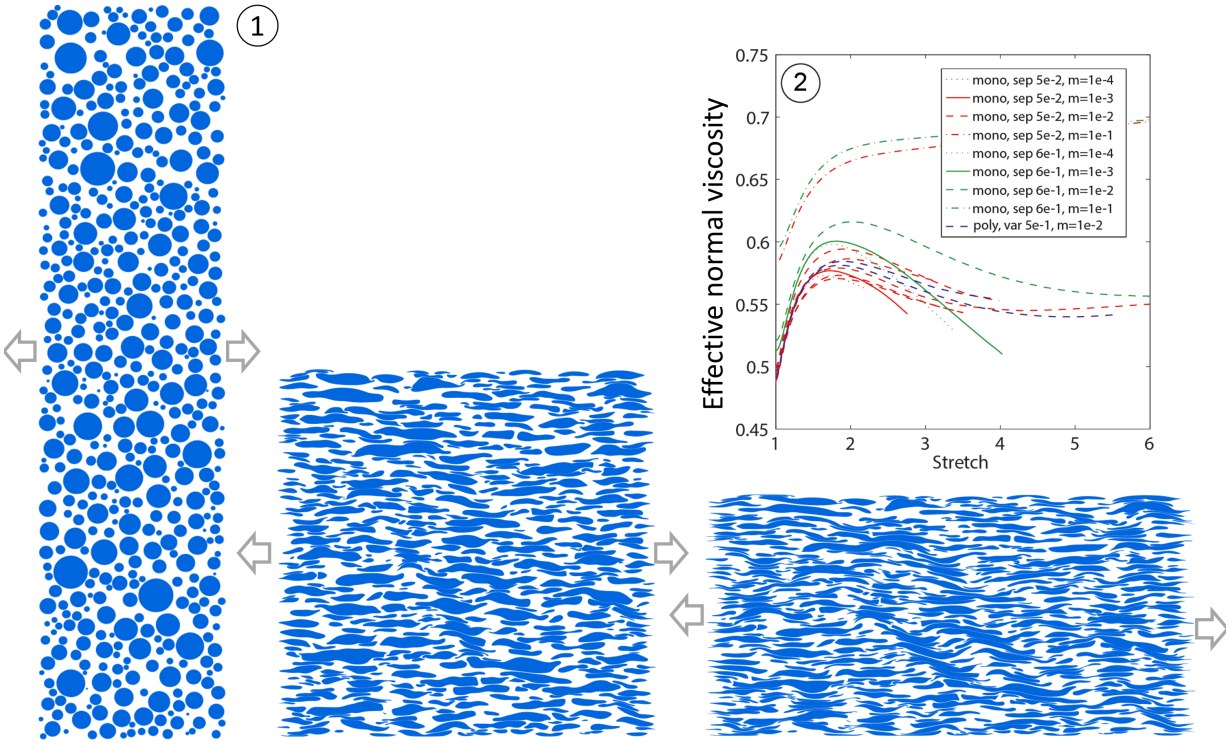

Fig. 1.: Fabric development in a poly-disperse inclusion-host composite subject to pure shear. Linear viscosity is used and the viscosity ratio was set to 1e-2. The inclusion fraction is 30% and the coefficient of variation of the log-normal distribution used for inclusion diameters was set to 0.5. 2) The effective normal viscosity normalized by the host viscosity as a function of stretch. The inclusion fraction is 30%. sep: minimum initial separation among the inclusions (scaled upon the smaller of the local radii), var: the coefficient of variation of the log-normal distribution, m: viscosity ratio between the inclusions and the host

random, statistically homogeneous (no clustering) and isotropic. In a series of complementary simulation runs, periodic inclusion arrays are analyzed. Both the inclusion and host materials are considered as viscous fluids and the intrinsic viscosities of the inclusion and the host phases are isotropic. A coherent inclusion-host interface is assumed and interfacial processes such as surface tension or diffusional mass transfer are neglected. The deformation is studied in the Stokes limit and under no gravity. A self-developed FEM code (www.milamin.org, Dabrowski et al., 2008) is used to find the velocity vectors at the inclusion interfaces. Unstructured triangular computational meshes adapting to or fitting all the internal inclusion boundaries are used in the simulations. To achieve the necessary resolution of the complex geometry of evolving inclusion-host interfaces, a large number of computational points is required. A test case is presented to demonstrate the performance of different ODE solvers and the accuracy of competing geometrical representations.

Results

Figure 1 shows that subjecting a two-phase composite consisting of weak inclusions (the viscosity

ratio of 1e-2) to pure shear deformation results in the development of stretched inclusions with complex sigmoidal shapes organizing into conjugate bands, which gives an overall impression of a structure resembling internal boudinage. The system undergoes hardening in the initial stages of stretching (the blue curves in the inset plot in Fig. 1). This behavior can be attributed to the development of shape preferred orientation, which results in an effectively anisotropic viscosity. The harderning phase is followed by an overall weakening phase, which can be correlated with the development of internal boudinage-like structures. The weakening phase occurs both in mono- and polydisperse composites. The peak of the hardening phase increases with increasing the initial separation between the inclusions. No weakening phase is observed for the viscosity ratio of 1e-1. A significant increase in the rate of weakening is observed with decreasing the viscosity ratio from 1e-2 to 1e-3.

References

Dabrowski, M., Krotkiewski, M., and Schmid, D. W. MILAMIN: MATLAB-based finite element method solver for large problems, Geochem. Geophys. Geosyst., 9, Q04030, 2008

Dabrowski, M., Schmid, D.W. and Podladchikov, Y.Y. A two-phase composite in simple shear: Effective mechanical anisotropy development and localization potential. Journal of Geophysical Research 117, 2012

Numerical models of ductile roots of mature strike-slip faults

Yuri Fialko[1]

[1] *Insitute of Geophysics and Planetary Physics, Scripps Insitution of Oceanography, University of California San Diego, La Jolla, CA 92093, USA*
e-mail: *yfialko@ucsd.edu*
session: *Rheolohy*

The degree to which strain is localized in the ductile part of the lithosphere below major faults is a major unresolved question in continental tectonics. Two classes of models have been proposed: one postulating a broadly distributed viscous deformation in the lower crust and upper mantle (the "thin lithosphere" model), and another one postulating extension of localized shear well below the brittle-ductile transition (the "thick lithosphere" model). Understanding the mechanics of lithospheric shear zones is essential for a number of problems in continental tectonics, including the long-term strength of the Earth's crust and upper mantle, stress transfer from the relative plate motion to seismogenic faults, and, ultimately, seismic hazards. Geological and geophysical evidence has been presented in support of both the "thin" and "thick" lithosphere models, possibly indicating differences in deformation styles between various locations, tectonic settings, deformation rates, and total displacements. If such variability exists, it is of interest to establish the main controlling factors and governing mechanisms on the observed deformation styles.

We investigate the long-term deformation and strain evolution due to major strike-slip faults in the continental crust. In particular, we use numerical models to evaluate the efficiency of various strain-softening mechanisms, such as thermomechanical coupling, grain-size reduction, and mylonitic fabric, and assess the degree to which they promote or inhibit strain localization, individually and in combination, in response to long-term fault slip. This is accomplished using finite element models that incorporate realistic geotherms, far-field loading rates and loading histories, depth-dependent compositions, and constitutive relationships inferred from laboratory experiments. Our simulations investigate conditions under which permanent shear zones may develop in an initially unstrained ductile substrate. We evaluate the magnitude and distribution of deviatoric stresses in the ductile lower crust and upper mantle, and make inferences about the long-term strength of continental lithosphere as a function of temperature regime, composition, deformation rate, total displacement, and other relevant factors. Observables that are brought to bear on the model predictions include grain size distributions from the exposed mid-to-lower crustal shear zones, inferences of deviatoric stress from petrologic and micro-structural data, seismic structure and anisotropy below active fault zones, and geodetic observations of transient and secular deformation due to major strike-slip faults.

The degree of strain localization in the ductile substrate depends on a number of factors such as the host rock composition, water content, geothermal gradient, and fault slip rate. Stiffer rheologies, lower ambient temperatures, and higher slip rates give rise to narrower shear zones. For the "San Andreas- ike" parameters used in our models, the predicted width of the thermally induced shear zone in the lower crust is of the order of a few km (*Takeuchi and Fialko*, 2012). Thus

much of the relative plate motion is accommodated by a "deep fault root" that extends into the lower crust, and further down into the upper mantle.

In models of (*Takeuchi and Fialko*, 2012), the behavior of the ductile substrate was governed by the constitutive relation for temperature- and stress- ependent power law dislocation creep. In these models, the thermally-activated power-law rheology was used as a proxy for all strain-weakening mechanisms. Such an approach does take into account diffusion creep, provided that contributions of dislocation creep and diffusion creep to the total strain rate are approximately equal (e. g., *De Bresser et al.*, 1998). We have also experimented with including into our models two additional mechanisms of ductile deformation that may be important in the lower crust and/or the upper mantle: grain size reduction and mylonitic fabric.

Grain size reduction

Grain size evolution is included in the viscous constitutive equation through the addition of grain size-dependent diffusion creep,

$$\dot{\varepsilon}_{diff} = A_{diff} d^{-m_{diff}} \sigma^{n_{diff}} \exp(-\frac{Q_{diff}}{RT}) \quad (1)$$

where d is grain size, n_{diff}=1, and A_{diff}, Q_{diff}, and m_{diff} are empirically determined parameters. Grain size reduction has been proposed as one of the mechanisms that can give rise to ductile shear zones observed in nature [e. g., *Fitz Gerald and Stüunitz* , 1993; *Jin et al.*, 1998] and laboratory experiments [e. g., *Tullis and Yund*, 1985; *Rutter* , 1995]. The grain size d is allowed to vary through a combination of static grain growth

$$\dot{d}_{+} = p^{-1} d^{1-p} G_0 exp(\frac{-H}{RT}) \quad (2)$$

and dynamic recrystallization

$$\dot{d}_{-} = -\lambda d \dot{\varepsilon}_{dis} \quad (3)$$

where G,p, and λ are empirical constants [*Hall and Parmentier*, 2003]. The constitutive equation for grain size evolution may either reflect a balance between the static grain growth and dynamic recrystallization [*De Bresser et al.*, 1998; *Montéesi and Hirth*, 2003; *Hall and Parmentier*, 2003], or evolution of the grains towards a stress-dependent equilibrium grain size $D = D_0 \sigma^{-r}$ where D_0 and r are material properties [*Van Der Wal et al.*, 1993; *Braun et al.*, 1999].

Grain size reduction may also be included with the addition of the grain size-dependent grain boundary sliding deformation mechanism. Grain boundary sliding allows for non-linear stress dependence similar to that of dislocation creep, while also allowing for grain size dependence similar to diffusion creep [*Hirth and Kohlstedt*, 1995]. Laboratory experiments have shown that deformation by grain boundary sliding is governed by a flow law similar to that of dislocation/diffusion creep [[*Hirth and Kohlstedt*, 1995; *Hansen et al.*, 2011].

$$\dot{\varepsilon}_{GBS} = A_{GBS} d^{-m_{GBS}} \sigma^{n_{GBS}} \exp(-\frac{Q_{GBS}}{RT}) \quad (4)$$

where A_{GBS}, n_{GBS}, Q_{GBS}, and m_{GBS} are empirically determined. Grain size evolution within the grain boundary sliding regime is governed by the same combination of static grain growth and dynamic recrystallization as described above.

Each of the three potential deformation mechanisms (dislocation creep, diffusion creep, and grain boundary sliding) may contribute to the total viscous strain rate,

$$\dot{\varepsilon}_{total} = \dot{\varepsilon}_{dis} + \dot{\varepsilon}_{diff} + \dot{\varepsilon}_{GBS}. \quad (5)$$

which requires only that constitutive parameters for each regime (readily available in references cited above) are defined to control the evolution of strain as a function of stress, temperature, and grain size during model execution.

Mylonitic fabric

We also assess the efficiency of fabric development due to large strains that give rise to differentiation of mineral phases and laminated textures, as observed in the exposed mylonite zones (*Berthe et al.*, 1979; *Büurgmann and Dresen*, 2008; *Mehl*

and Hirth, 2007; *Sibson*, 1978). The net result is formation of quasi-continuous layers of different mineral composition. Creep rate of each mineral phase is governed by equation 5 (any combination of deformation regimes may again be assumed). The total strain rate for a given volume of rock of multi-phase composition (or finite element, in case of a numerical model) is a volume-weighted superposition of the individual strain rates for each phase

$$\dot{\varepsilon}_{total} = \sum_{i=1}^{N} \dot{\varepsilon}_i \phi_i; \qquad \sum_{i=1}^{N} \phi_i = 1 \tag{6}$$

where ϕ_i are the volume proportions of the various phases, respectively [*Handy*, 1994].

In our models, we use a constitutive relationship for a laminated material, in which bands of a rheologically weak phase are interspersed within bands of stronger phases. Under a given applied shear stress, the total strain across a given volume of rock is insensitive to the details of band spacing, as long as the volume proportions of each phase are preserved. For example, for a two-phase mylonite composed of a weak phase and a strong phase subjected to a shear stress parallel to foliation, the total velocity across a 2-band layer having thickness $x + y$, where x is the thickness of a weak phase and y is the thickness of a strong phase, is identical to the velocity across the layer of the same thickness, composed of 10 weak and 10 strong bands having individual thicknesses of $0.1x$ and $0.1y$, respectively. One can then compute the total strain rate for a given volume as

$$\dot{\varepsilon}_{total} = \dot{\varepsilon}_w \phi_w + \dot{\varepsilon}_s \phi_s + \dot{\varepsilon}_a \phi_a \tag{7}$$

where ϕ_w and ϕ_s are the volume proportions of the weak and strong phases, respectively, and ϕ_a is the volume proportion of the aggregate rock. To illustrate this formulation, we use laboratory-derived constitutive relations for synthetic anorthite-diopside aggregates (*Dimanov and Dresen*, 2005), which have been used as a proxy for lower crustal rocks of gabbroic composition (e. g., *Mehl and Hirth*, 2007). *Dimanov and Dresen* (2005) presented dislocation and diffusion creep flow law parameters (equation 5) for pure anorthite, pure diopside, and two-phase mixtures with various volume proportions of each phase. Using these parameters, we calculate the effective viscosity of the phases for a given stress and temperature.

Figure 1 shows the distribution of velocity across a simulated volume of a material comprised of three different laminated rheologies; 0-10 cm: 5 cm pure wet anorthite and 5 cm pure wet diopside (fully laminated rheology- ϕ_w=0.5, ϕ_s=0.5, ϕ_a=0); 10-20 cm: 2.5 cm pure wet anorthite, 2.5 cm pure wet diopside, 5 cm wet 50% anorthite-50% diopside mixture (partially laminated rheology- ϕ_w=0.25, ϕ_s=0.25, ϕ_a=0.5); 20-30 cm: 10 cm wet 50% anorthite-50% diopside mixture (unlaminated rheology- ϕ_w=0, ϕ_s=0, ϕ_a=1), subjected to a shear stress of 10 MPa and a temperature of 500°C. Though the total composition of the rock (50% anorthite and 50% diopside) is preserved within each 10 cm band, greater deformation occurs in regions with high volume proportions of weak anorthite. If we assume that the volume proportions for each phase vary either (i) as a function of distance from the fault (time-invariant distribution) or (ii) as of function of total strain (in this case, the volume proportions would evolve during the simulation), deformation will localize in proportion to the degree of phase separation.

Figure 2 shows preliminary simulations that include the effects of thermomechanical coupling and grain size evolution. Subplots (a)-(c) in Figure 2 illustrate strain rates through 10 Myr of deformation, under the same boundary conditions as described above. The model consists of a 12 km thick elastic crust underlain by a ductile substrate that deforms by a combination of dislocation and diffusion creep. For simplicity, we assume the rheology of a wet olivine ($A_{dis} = 3.6e5$ $\mathrm{MPa}^{-3.5}\mathrm{s}^{-1}$; $n_{dis} = 3.5$; $Q_{dis} = 480e3$ kJ mol^{-1}; $A_{diff} = 1e9$ $\mathrm{MPa}^{-1}\mathrm{s}^{-1}$, $n_{diff} = 1$; $Q_{dis} = 335e3$ kJ mol^{-1}; A_{dis} and A_{diff} have a constant water content C_{OH} = 1000 H/10^6Si folded in, [*Hirth and Kohlstedt*, 2003; *Freed and Büurgmann*, 2004]) for the entire substrate. Strain localization occurs in these models by (a) grain size evolution

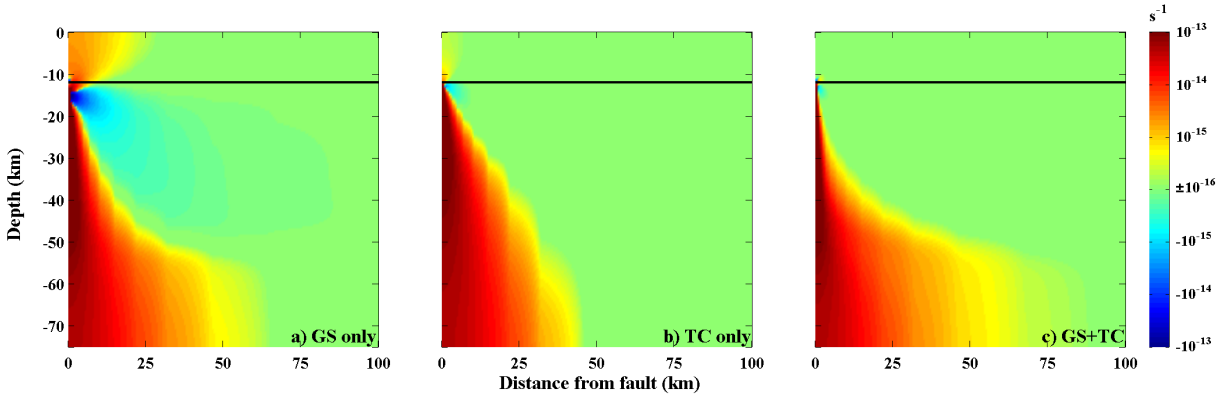

Fig. 2.: Preliminary results from a coarse-meshed model showing strain rate vs. depth and distance from fault through 10 Myr of simple shear. a) Grain size evolution (diffusion and dislocation creep); b) thermomechanical coupling (dislocation creep only); c) grain size evolution and thermomechanical coupling (diffusion and dislocation creep). Solid black line denotes the elastic-viscoelastic transition at 12 km depth.

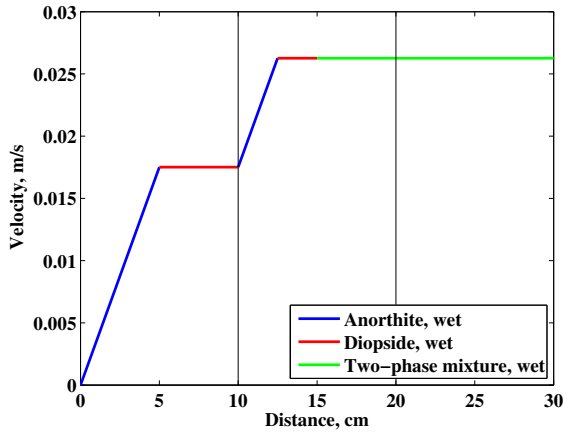

Fig. 1.: Distribution of velocity across a 30 cm-thick layer of simulated material composed of three laminated rheologies: 0-10 cm: 5 cm pure wet anorthite (blue) and 5 cm pure wet diopside (red); 10-20 cm: 2.5 cm pure wet anorthite (red), 2.5 cm pure wet diopside (blue), 5 cm wet 50% anorthite-50% diopside mixture (green); 10 cm wet 50% anorthite-50% diopside mixture (green), subjected to a shear stress of 10 MPa at a temperature of 500°C. All phases deform by dislocation creep, with flow law parameters from *Dimanov and Dresen* (2005).

($p = 3$; $G_0 = 4.3e-1$ m^{3}s^{-1}; $H = 600$ kJ mol^{-1}; $\lambda = 1$, equations 2 and 3 [*Hall and Parmentier*, 2003], assuming deformation by diffusion and dislocation creep); (b) shear heating and thermomechanical coupling, assuming deformation by dislocation creep only; and (c) a combination of grain size evolution and thermomechanical coupling, assuming deformation by diffusion and dislocation creep. All models assume an initial geotherm of 20°C/km. The initially one-dimensional temperature field is modified by shear heating and heat conduction in models (b) and (c). Initial grain sizes are 1 mm for models (a) and (c). Each model exhibits development of a shear zone below the elastic layer, with most intense strain located within 30 km of the fault plane (horizontal coordinate of 0). Models incorporating grain size evolution (a and c) show a significant delocalization of deformation towards the bottom of the domain, owing to the relatively high temperatures and enhanced grain growth (equation 2) at depth. Notably, the model combining grain size evolution and thermomechanical coupling (model c) shows robust localization within ∼3 km of the fault plane in the depth interval ∼12-30 km. Localization in this region is more pronounced relative to that in models accounting for the grain size evolution or thermomechanical coupling alone (Figure 3). In fact, the degree of strain localization in this case appears to be

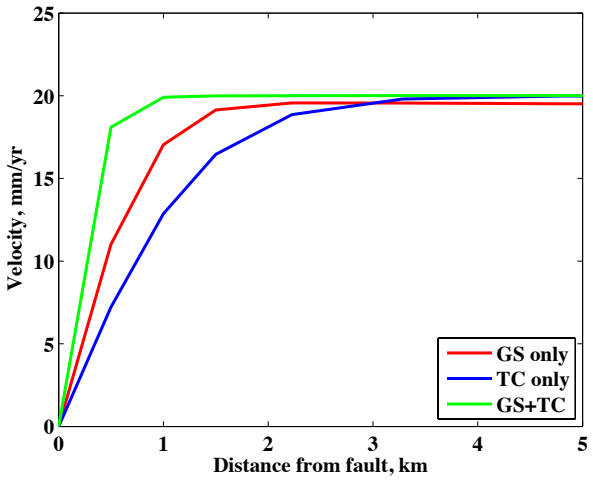

Fig. 3.: Profiles of fault-parallel velocity at depth of 20 km, for the deformation mechanisms illustrated in Figure 2: grain size evolution (red line), thermomechanical coupling (blue line), and a combination of the grain size evolution and thermomechanical coupling (green line).

limited by the mesh size, and we expect it to be even more pronounced upon a suitable mesh refinement. Our preliminary results shown in Figures 2 and 3 suggest that thermomechanical coupling and grain size reduction can work in concert to enhance strain localization in the lower crust and the upper mantle.

References

Handy, M., Flow laws for rocks containing nonlinear viscous phases: a phenomenological approach, J. Struct. Geol., 16, 287-301, 1994.

Hansen, L., M. Zimmerman, and D. Kohlstedt, Grain boundary sliding in San Carlos olivine: Flow law parameters and crystallographic-preferred orientation, J. Geophys. Res., 116, B08201, doi:10.1029/2011JB008220, 2011.

Hirth, G., and D. Kohlstedt, Experimental constraints on the dynamics of the partially molten upper mantle 2. Deformation in the dislocation creep regime, J. Geophys. Res., 100, 15,441-15,449, doi:10.1029/95JB01292, 1995.

Hirth, G., and D. Kohlstedt, Rheology of the upper mantle and mantle wedge: A view from the experimentalists, in Inside the Subduction Factory, Geophys. Monogr. Ser., vol. 138, edited by J. Eiler, pp. 83-105, AGU, Washington, D. C, 2003.

Jin, D., S.-I. Karato, and M. Obata, Mechanisms of shear localization in the continental lithosphere: Inference from the deformation microstructures from the Ivrea zone, Northwest Italy, J. Struct. Geol., 20, 195-209, 1998.

Mehl, L., and G. Hirth, Plagioclase preferred orientation in layered mylonites: Evaluation of ow laws for the lower crust, J. Geophys. Res., 113, B05202, doi:10.1029/2007JB005075, 2007.

Montéesi, L., and G. Hirth, Grain size evolution and the rheology of ductile shear zones: From laboratory experiments to postseismic creep, Earth Planet. Sci. Lett., 211, 97-110, doi:10.1016/S0012-821X(03)00196-1, 2003.

Rutter, E., Experimental study of the in uence of stress, temperature, and strain on the dynamic recrystallization of Carrara marble, J. Geophys. Res., 100, 24,651-24,663, doi:10.1029/95JB02500, 1995.

Sibson, R., Fault rocks and fault mechanisms, Journal of the Geological Society, 133, 191-213, 1978.

Takeuchi, C., and Y. Fialko, Dynamic models of interseismic deformation and stress transfer from plate motion to continental transform faults, J. Geophys. Res., 117, B05403, doi:10.1029/2011JB009056, 2012.

Tullis, J., and R. Yund, Dynamic recrystallization of feldspar: A mechanism for ductile shear zone formation, Geology, 91, 238-241, 1985.

Van Der Wal, D., P. Chopra, M. Drury, and J. Fitz Gerald, Relationships between dynamically recrystallized grain size and deformation conditions in experimentally deformed olivine rocks, Geophys. Res. Lett, 20, 1,479-1,482, doi:10.1029/93GL01382, 1993.

Present-day intra-plate deformation of the Eurasian plate

Candela Garcia-Sancho[1], Rob Gover[1], Karin N. Warners-Ruckstuhl[2], Magdala Tesauro[1]

[1] *Utrecht University, Faculty of Geosciences, Earth Science Dept, Utrecht, The Netherlands*
[2] *Shell Global Solutions, Kesslerpark 1, 2288 GS, Rijswijk, The Netherlands*
e-mail: *C.GarciaSancho@uu.nl*
session: *Rheology*

We build on the results of two recent, yet independent, studies. In the first (Warners-Ruckstuhl et al., 2013) the forces on, and stresses within the Eurasian plate were established. In the second (Tesauro et al., 2012) the distribution of mechanically strong and weak parts of the Eurasian plate was found. The aim of our work is to predict lithospheric deformation of the Eurasian plate and to compare it with observations. This constitutes a test of both the force/stress results and of the strength results. Specific questions are to which extent stresses localize in specific regions and whether micro-plates as identified by geodesists arise naturally from the results.

Importantly, Warners-Ruckstuhl et al. (2013) found an ensemble of mechanically consistent force models based on plate interaction forces, lithospheric body forces and convective tractions. Each of these force sets is in mechanical equilibrium. A subset drives Eurasia in the observed direction of absolute motion and generates a stress field in a homogeneous elastic plate that fits observed horizontal stress directions to first order (Fig 1.). Deformation models constitute a further test and a possibility to discriminate between the remaining force sets.

Following Tesauro et al. (2012) we assume five different compositions for the upper and lower crust according to the age of the geological provinces (Fig 2.). We use their geotherms and crustal thickness maps to estimate vertical distributions of strength at any location within the Eurasian plate. We compute de vertical distribution of strength for each element of the domain, and integrate it up to the value of the previously calculated stress field to obtain the lithospheric strength of each element of the model.

From the power-law relationship between strength and viscosity, and based on the assumption that horizontal strain rates do not vary with depth, we estimate the vertically averaged viscosity of each element of the domain.

We compute deformation in our model by solving the mechanical equilibrium equation using finite element code GTECTON. It is computed in a spherical shell using plane stress approximation. We plan to include major active faults in our mechanical model.

We compare our results with GPS velocities, InSAR, seismic, and paleomagnetic observations, which capture present-day and long-term deformation. We discuss various causes for differences.

References

Warners-Ruckstuhl et al., Tethyan collision forces and the stress field of the Eurasian plate, Geophys.J.Int., 219, 2013.

Tesauro et al., Global strength and elastick thickness of the lithosphere, Global Plan. Chang., 90-91, 51-57, 2012.

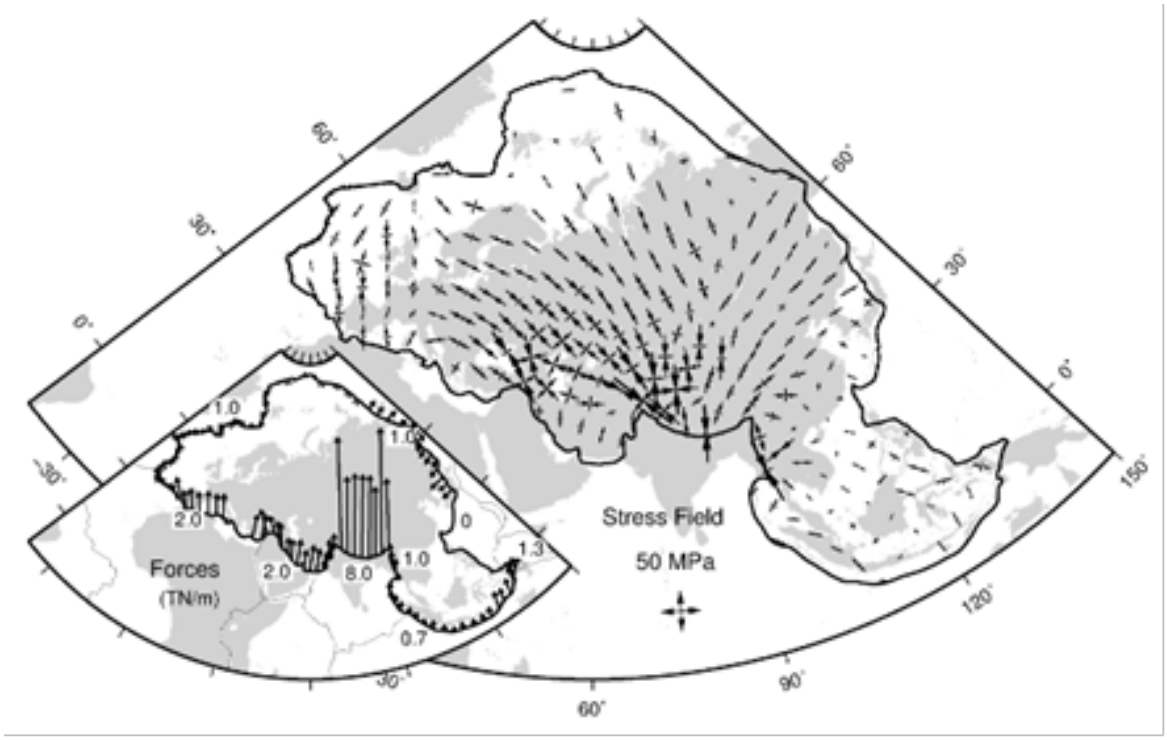

Fig. 1.: Principal axes of the stress field (MPa). Corresponding average edge forces are displayed in the inset (TN/m).

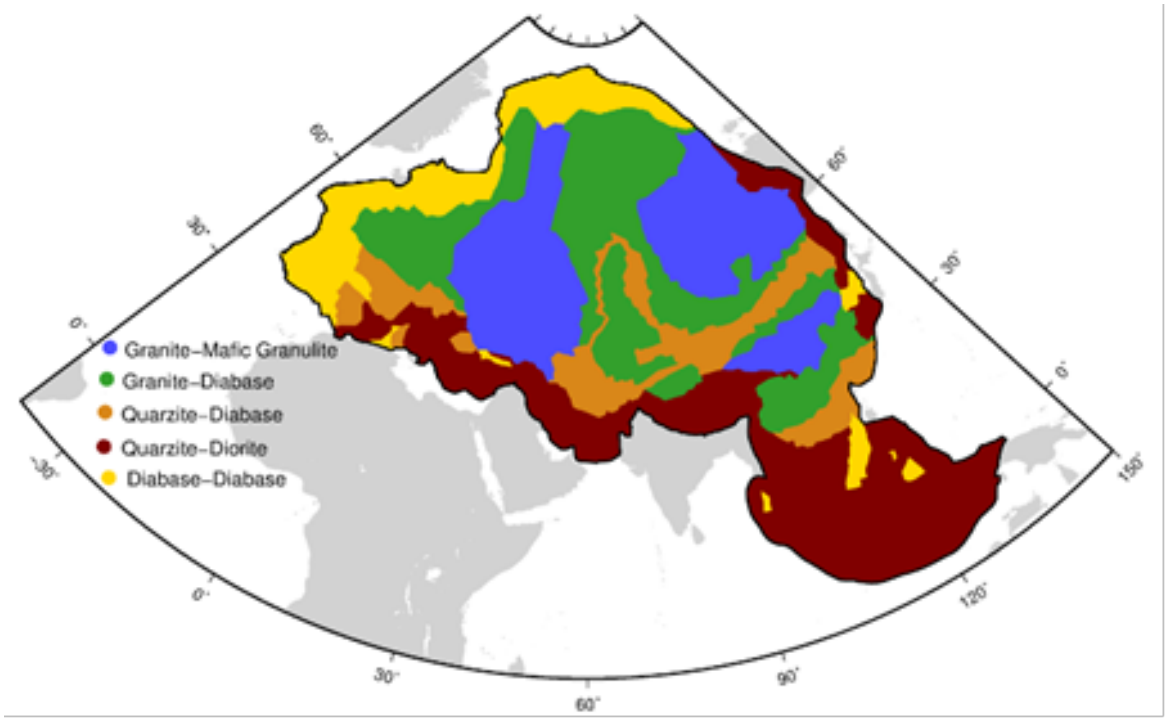

Fig. 2.: Eurasia composicioal types of the upper and lower crust over dry olivine lithospheric mantle

Localization of deformation in a polymineralic material

Suzon Jammes[1], Luc L. Lavier[1], Jacqueline E. Reber[1]

[1]*Institute for Geophysics, University of Texas at Austin, USA*
e-mail: *suzon.jammes@austin.utexas.edu*
session: *Rheology*

Even though ninety-five volume percent of all rocks are polymineralic, metric and crustal scale numerical experiments mainly used monomineralic material composed of wet or dry, plagioclase, quartz or olivine to approximate rock behavior. This approach presumes that the rheology of the crust or mantle is mainly controlled by the weakest or the most abundant mineral phase. An assumption that can be debated in regards to experimental and theoretical studies realized on bimineralic and polymineralic rocks, which show that their bulk strength depends also on the proportion, shape, distribution, and strength ratio of the minerals [Handy, 1990; Jordan, 1988]. Moreover, since the transition from brittle to ductile deformation depends on the individual brittle ductile transition of each mineral phase it is expected that under certain conditions some deform brittle while others show ductile deformation. Natural observations show that minerals that are harder than their surrounding matrix tend to remain as only slightly deformed porphyroclasts or that they can exhibit localized fractures while the rest of the material presents evidence of ductile deformation [Mitra, 1978; Wakefield, 1977; White et al., 1980], inferring that a mixed brittle-ductile or semi-brittle rheology is at play.

Evidence for such a behavior can be observed in a wide range of examples at different length scales (from microscopic to crustal scale) and in different types of materials such as quartzofeldspatic rocks [Tullis et al., 2000] or olivine rich mantle rocks in the presence of serpentine or plagioclase [Kaczmarek and Müntener, 2008]. All these observations suggest that a polymineralic composition has a strong influence on deformation processes and localization of the deformation from the microscopic to the lithospheric scale.

Here, we consequently investigate the relation between polymineralic composition and localization of the deformation. To simplify our experiments and to reduce the number of parameters, we perform metric scale numerical models with a bimineralic composition using shearing boundary conditions leading to a fracture-like localization at different temperatures and strain rates (Figure 1). With this approach we seek to answer: how does localization occur in bi-mineralic materials? What impact has the percentage of weak versus strong phase on the localization of the deformation? And how does the temperature and strain rate, controlling the strength difference between the two minerals, affect the localization and deformation processes?

This study shows that the deformation localization is highly dependent on the fraction of the weak phase as well as the strength ratio between the phases. We identify four domains where the deformation can be characterized as brittle, semi-brittle, semi-ductile, or ductile depending on the mechanical behavior and strength ratio between the two phases. Similar to Handy [1990]'s classification, we define three deformation types to characterize the degree of localization within the shear zone. Type I deformation is controlled by the strong phase. In presence of a weak phase, the strong phase forms an interconnected load bearing framework surrounding the weak phase and deformation is accommodated along a straight and thin shear zone. Type II is characterized by the formation of anastomosing structures controlled by the distribution of the weak phase while

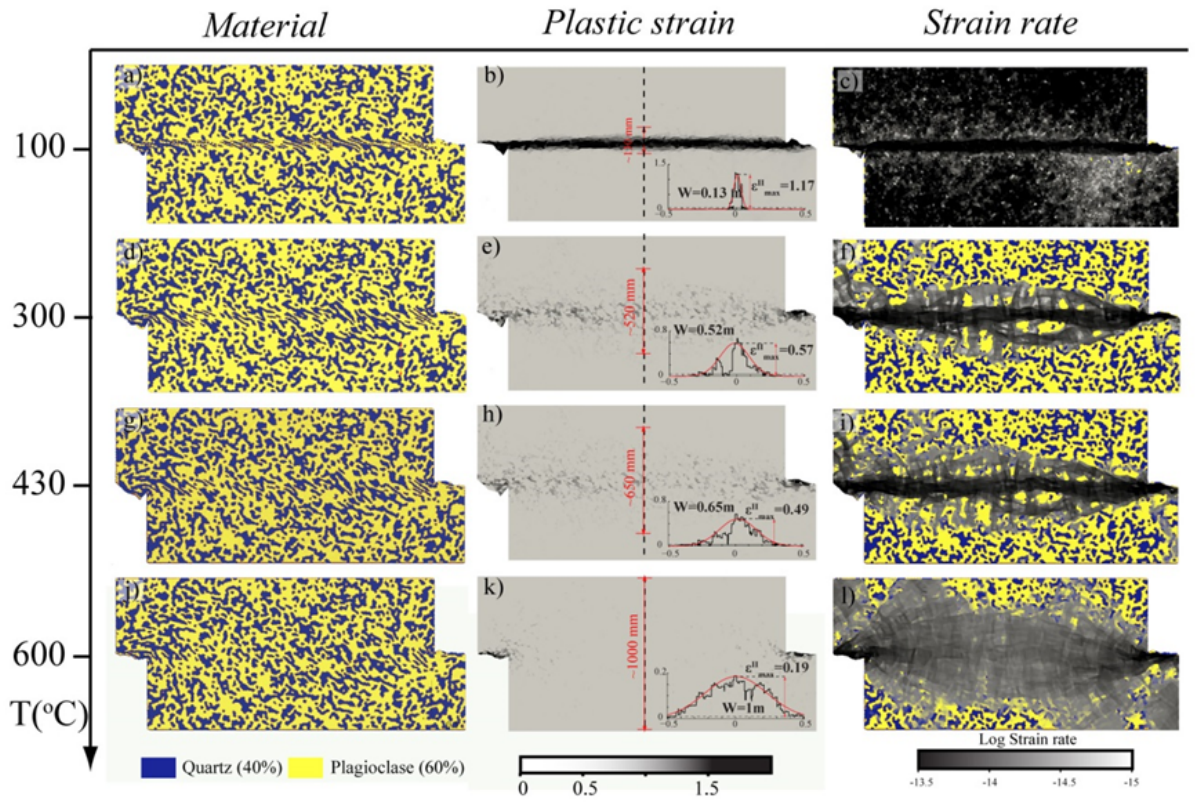

Fig. 1.: Example of a numerical experiment realized for a concentration of quartz equal to 40% with a temperature set at: a-c) 100 °C, d-f) 300 °C, g-i) 430 °C and j-l) 600 °C. Left: material distribution. Middle: Distribution of the accumulated plastic strain. The inset in the right bottom corner of each model shows the distribution of the second invariant of the strain or effective strain (ϵ^{II}) with a corresponding Gaussian approximation along a cross-section through the central part of the model, an estimation of the maximum value of ϵ^{II}_{max} and the width of the shear zone (W). Right: Representation of the logarithmic value of the strain rate when strain is equal to 0.2 superimposed on the material distribution.

the strong phase forms elongated augen; the significant strain in both phases indicates that they are both rheologically active. In type III the strong phase forms relatively undeformed clasts in a weak matrix and is consequently inferred to be rheologically passive and a delocalized shear zone can be observed.

Our results are summarized in the Figure 2 where we correlate the depth dependent strength profile of wet quartz and plagioclase (the reference strain rate is equal to 10-14 s-1) (Figure 2a) to a phase diagram showing the different deformation types observed in the numerical experiments depending on the quartz concentration (Figure 2b). This correlation between the deformation types and the different domains allows us to determine the impact of the phase ratio and the strength ratio on the shear localization. The results can be resumed as follow. At low temperature (brittle domain) both mineral behave in a brittle manner and a narrow shear zone forms (Type I). In the semi-brittle domain, one mineral phase deforms in a brittle manner and the other deforms ductily and all three types of deformation can be observed depending of the amount of the weak phase. If the weak phase ratio is low enough the deformation is mainly brittle (Type I) whereas anastomoses occurs (Type II) when the amount of weak phase increases. For a high weak phase ratio the shear zone is fully ductile, the shear zone is very wide and no deformation of the strong mineral phase is occurring (Type III). In

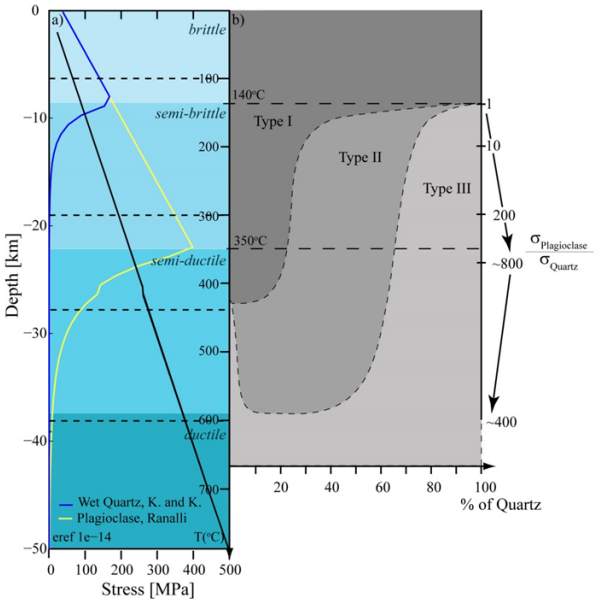

Fig. 2.: a) Depth dependent strength profile of wet quartz and plagioclase calculated for a reference strain rate equal to 1e-14. b) Phase diagram showing the different types of deformation observed in the numerical experiments depending on the quartz concentration, the temperature and corresponding strength ratio between the two phases.

the semi-ductile domain, both mineral phases are expected to behave in a ductile manner. However, contrary to what is expected from the dislocation creep law, plagioclase still exhibits brittle behavior in presence of quartz and therefore displays the characteristics of type II deformation. For a high amount of quartz both phases are behaving in a ductile manner leading to the formation of a wide shear zone (Type III). Fully ductile deformation independent of the weak phase ratio (Type III) only occurs for high temperatures.

Finally, this study demonstrates that in the semi-ductile domain deformation in monomineralic rocks (0% of quartz) is strongly delocalized (Type III) whereas in polymineralic rocks, with the addition a small amount of weak phase, the deformation will localize with an intensity depending on the amount of the weak phase (Type II). It appears therefore that the insertion of a small amount of weak phase can revert the mechanical behavior of the strong phase and lead to the formation of a narrow semi-brittle shear zone (Type II) where a fully ductile (Type III) behavior is expected. This highlights the importance of a bi-mineralic material on the deformation localization and furthermore on large scale deformation processes.

References

Handy, M. R. (1990), The solid-state flow of polymineralic rocks, Journal of Geophysical Research: Solid Earth (1978–2012), 95(B6), 8647-8661.

Jordan, P. (1988), The rheology of polymineralic rocks - an approach, Geologische Rundschau, 77(1), 285-294.

Kaczmarek, M.-A., and O. Müntener (2008), Juxtaposition of melt impregnation and high-temperature shear zones in the upper mantle; field and petrological constraints from the Lanzo Peridotite (Northern Italy), Journal of Petrology, 49(12), 2187-2220.

Mitra, G. (1978), Ductile deformation zones and mylonites; the mechanical processes involved in the deformation of crystalline basement rocks, American Journal of Science, 278(8), 1057-1084, doi:10.2475/ajs.278.8.1057.

Tullis, J. A., H. Stünitz, C. Teyssier, and R. Heilbronner (2000), Deformation Microstructures in Quartzo-feldspathic Rocks, in Stress, Strain and Structure, A volume in honour of W D Means, edited by M. W. Jessell and J.L.Urai., Journal of the Virtual Explorer.

Wakefield, J. (1977), Mylonitization in the Lethakane shear zone, eastern Botswana, J. geol. Soc. Lond., 133, 262-275.

White, S., S. Burrows, J. Carreras, N. Shaw, and F. Humphreys (1980), On mylonites in ductile shear zones, Journal of Structural Geology, 2(1), 175-187.

Localization processes on Earth, Mars, and Venus

Laurent G.J. Montési[1], Frédéric Gueydan[2]

[1] *University of Maryland, Department of Geology, USA*
[2] *Université Montpellier 2, Géosciences Montpellier, France*
e-mail: *montesi@umd.edu*
session: *Rheology*

Introduction

Few problems in Earth Science are as fundamental as the origin of plate tectonics. Our planet has adopted a global tectonic regime that appears unique in the solar system [1]. A fundamental characteristic of plate tectonics is that deformation is localized in narrow deformation zones. As strike-slip faults in particular do not contribute to removing heat from the interior of the planet, localized shear zones must instead act as zones of weakness [2]. Although weakness is often construed as a reduction in stress required to deform a rock at given strain rate, a more geological relevant definition of weakness is that the strain rate is higher than outside the shear zone, whereas stress is probably the same in the shear zone and in the host rock (at least in simple shear).

Localization seen as the consequence of weakening leads to an energy conundrum that can only be resolved is rock rheology depends on deformation history through a state variable. As ductile rheologies are fundamentally strain rate hardening, the high strain rate inside a narrow shear zone leads to higher energy dissipation rate than in a broad shear zone. Therefore, localization must involve a weakening process to make deformation in a localized more favored over distributed deformation [3].

I summarize here localization processes proposed to be active on Earth, their effect, and whether or not they may be active in other terrestrial bodies.

Efficiency of localization processes

Rocks deform following brittle processes at relatively shallow pressure and temperature and plastic mechanisms are greater depth. Geological observations on Earth show that deformation can localize under both conditions [4], even though plastic rheologies, being strain-rate hardening, are fundamentally stable in the laboratory [3, 5]. Localization can be understood in either case if a state variable enables rock strength to weaken as strain accumulates.

Brittle processes involve the formation of, and sliding along, cracks between and inside grains that form a rock. It is therefore not surprising that brittle failure should result in a localized shear zone. Additional processes that weaken brittle shear zones include nucleation of weak minerals like serpentine, graphite, and mica [6] and the development of a foliated cataclastic zone [7]. All these phenomena contribute to decrease the coefficient of friction from 0.6 to 0.1. A key to achieve such weakness is that fault gouge adopts a fabric that allows the weak phase to form a through-going layer [8].

Localization in the ductile regime is harder to understand, because of the fundamental strain-rate hardening behavior of plastic deformation process. Montési [5] describes how modifying a well-chosen state variable inside a narrow domain (the shear zone) can reduce the energy required for deformation, compensating for the high deformation rate in the shear zone. His method allows the localization of a localization potential that describe how narrow a shear zone can be

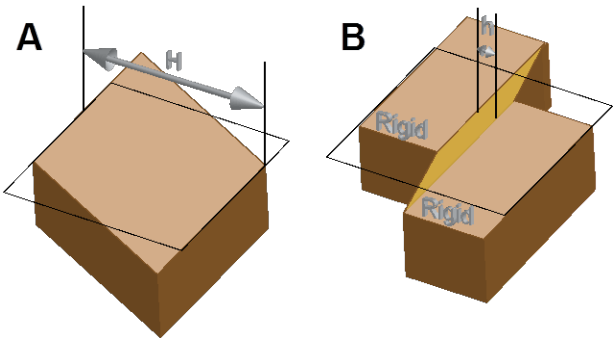

Fig. 1.: Schematics diagrams illustrating (A) the reference non-localized deformation state and (B) the localized states, where the different shade of the shear zone indicates a different temperature or microstructure. The localization potential $L = h/H$ is computed by comparing energy dissipation between configurations A and B (Montési, 2013).

produced by a change in state variable before it is no longer energetically favorable (Figure 1).

Only a few state variables are efficient enough to lead to localized deformation, at least if the change is limited to what is observed in geological example [5]. Other characteristics of shear zones should be regarded as consequences of the large strain in the shear zone but do not have a significant rheological effect.

The most efficient localization process active in the continental crust appears to be the development of a layered fabric. Ductile shear zones are formed of anastomosing high-strain bands at many scales [4, 9]. The high-strain zones are often rich in phyllosilicates, sometimes to the point of being classified as phyllonite. Development of a layered fabric enables the weakest phase to control the rheology of the deforming rock. If that phase is weak or highly nonlinear, like micas, pronounced weakening is associated with the appearance of a layered fabric [5]. This localization process is clearly limited to temperatures are which micas are stable ($\sim 450\,^{\circ}\mathrm{C}$).

In the mantle ductile shear zone rocks are often synonym with mylonites, i.e., they are characterized by a reduced grain size [10-13]. Reducing grain size is possible only when dislocations are active inside the rocks [e.g. 14]. However, it leads to weakening only if grain boundary sliding and diffusion are dominant. Therefore, grain size reduction is a viable localization process only in the dislocation-accommodated Grain Boundary sliding regime (dis-GBS, [15]). The mantle can localize in this regime at temperatures less than less than $800\,^{\circ}\mathrm{C}$ [16].

Application to terrestrial planets

The localization potential analysis described above reveals that localization is possible not only in the brittle levels of the lithosphere but also in the ductile regime at relatively low temperatures where either micas are present or dis-GBS is active (mantle at temperature less than $800\,^{\circ}\mathrm{C}$).

Applying this insight to the continental lithosphere, we see that localization can take place in the middle crust and uppermost mantle, but not in the lower crust that separates them. Gueydan et al. [16] developed from these constraints the concept of strain-dependent lithospheric strength. At low strain, the upper mantle and upper crust are the strongest regions of the lithosphere. However, fabric evolution reduces strength in the upper crust (brittle fabric), middle crust (fabric in presence of mica) and upper mantle (grain size reduction). The reduced strength of the lithosphere as a whole leads to increased strain rate if the loading stress, controlled by large-scale tectonics, does not change. The lower crust, which does not weaken, becomes the load-bearing layer at high strain. This model is able to reconcile different views of the lithospheric strength profile by associating the classic "jelly sandwich" model to low strain areas and the "crème brûlée" model to high strain areas [17].

It should be noted that the localizing uppermost mantle is expected to be absent in regions of thickened crust, like the Tibetan plateau, and regions with high heat flux, like the Basin and Range province of the Western United States. Accordingly, deformation remains diffuse in these regions.

The oceanic lithosphere is simple to understand as it does not require considering the complica-

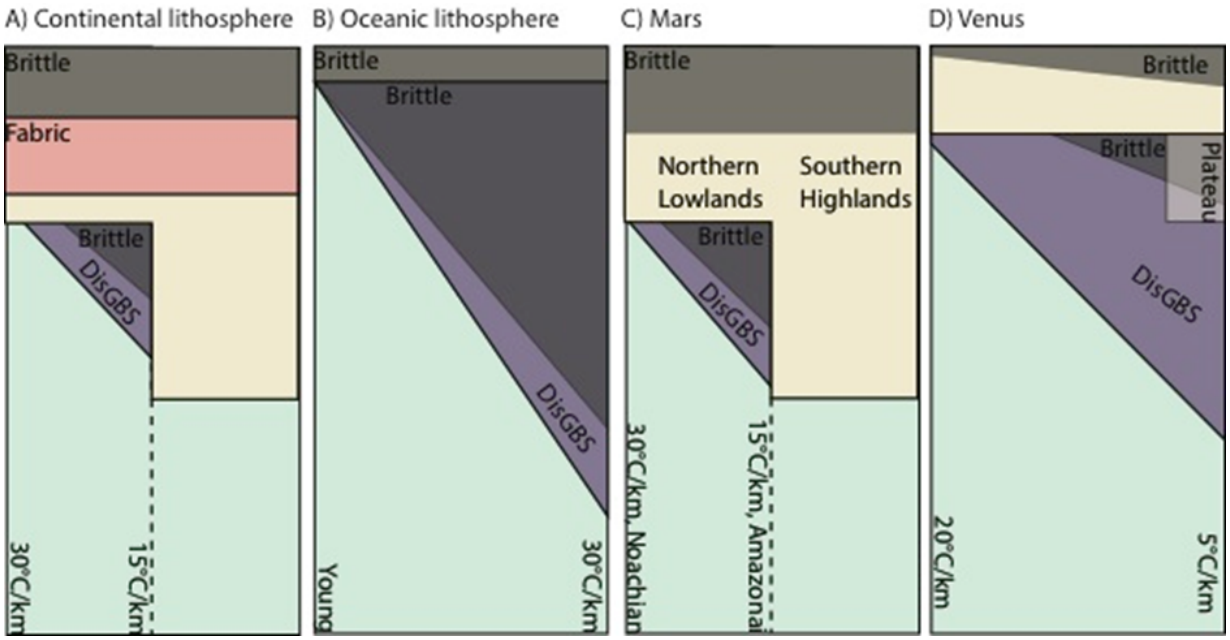

Fig. 2.: Representation of localization processes in planetary lithospheres. Green: mantle, no localization. Purple: mantle, localization by grain size reduction in presence of dis-GBS. Brown: crust, no localization. Pink: crust, localization by fabric development in presence of micas. The vertical axis represents depth with an approximate scale of 1.5mm/km. The horizontal axis corresponds to different tectonic environments or geotherm (as indicated).

tions of layer development in the crust. Localization is possible in a brittle lithospheric mantle with a thickness that increases with age. Dis-GBS lines the base of this brittle mantle but does not affect much the general organization of the lithosphere. It should be noted that it is in the oceans that the most localized shear zones are observed [2].

The rheological profile of Mars resembles that of the continental crust with brittle upper crust and upper mantle separated by a non-localizing lower crust. Here again, the localizing uppermost mantle is absent if the crust is too thick (Southern Highlands) or too hot. Ductile shear zone development is not expected in the crust because its basaltic composition [18] is not conducive to the presence of micas similar to those observed in terrestrial shear zones [19]. Therefore, the lower crust constitutes a more efficient impediment to failure of the lithosphere as a whole than it does on Earth. More importantly, the uppermost mantle can only be localizing only if the geotherm is less than 25 °C/km, which corresponds to the middle Hesperian period. By then, the convective vigor may have decreased below what is necessary for plate tectonics to form. The absence of plate tectonics in the Martian geological records may be ascribed to the disconnection between driving forces and localization potential over time.

Venus appears unlike the Earth in that localization can only occur in a thin brittle layer at the surface or in a thick region of the mantle where dis-GBS is active. If this mantle is able to generate localized shear zones, these may be sufficiently far from the surface that they do not have a evident effect on surface geology. Alternatively, it may be that brittle failure in contact with dis-GBS mantle is necessary to trigger localization and that otherwise the localization in the uppermost mantle is stabilized by interaction with adjoining non-localizing regions.

References

[1] O'Neill, C., Jellinek, A.M., Lenardic, A., (2007). Conditions for the onset of plate tectonics on terrestrial planets and moons, Earth and Planet. Sci. Lett. 261, 20– 32.

[2] Bercovici, D., Ricard, Y., Richards, M.A. (2000). The relation between mantle dynamics and plate tectonics: A primer. In: Richards, M., Gordon, R., van der Hilst, R. (Eds), The History and Dynamics of Global Plate Motions, Geophys. Monograph 121, 1–46.

[3] Montési, L.G.J., and Zuber, M.T. (2002), A unified description of localization for application to large-scale tectonics, J. Geophys. Res., 102, doi:10.1029/2001JB000465.

[4] Vauchez, A., A. Tommasi, and D. Mainprice (2012). Faults (shear zones) in the Earth's mantle, Tectonophysics 558-559, 1-27, doi: 10.1016/j.tecto.2012.06.006.

[5] Montési, L.G.J. (2013) Fabric development as the key for forming ductile shear zones and enabling plate tectonics, J. Struct. Geol. 50, 254–266.

[6] Lockner, D.A., et al. (2011). Low strength of deep San Andreas fault gouge from SAFOD core, Nature 472, 82-85.

[7] Collettini, C., A. et al., (2009), Fault zone fabric and fault weakness, Nature 462, 907-911.

[8] Rutter, E.H. et al. (2013). Reduction of friction on geological faults by weak-phase smearing, J. Struct. Geol. 51, 52-60, doi: 10.1016/j.jsg.2013.03.008.

[9] Gerbi, C., N. Culshaw, and J. Marsh (2010), Magnitude of weakening during crustal-scale shear zone development, J. Struct. Geol. 32, 107– 117.

[10] Drury, M.R. et al. (1991), Strain localization in upper mantle peridotites, Pure Appl. Geophys. 137, 439– 460, doi:10.1007/BF00879044 .

[11] Jin, D., S.-I. Karato, , and M. Obata (1998). Mechanisms of shear localization in the continental lithosphere: Inference from the deformation microstructures from the Ivrea zone, Northwest Italy, J. Struct. Geol. 20, 195– 209.

[12] Precigout, J., and F. Gueydan (2009), Mantle weakening and strain localization: Implications for the long-term strength of the continental lithosphere, Geology, 37, 147-150. doi:10.1130/G25239A.1.

[13] Platt J. P., and W. M. Behr (2011). Grainsize evolution in ductile shear zones: Implications for strain localization and the strength of the lithosphere.= J. Struct. Geol. 33, 537– 550, doi:10.1016/j.jsg.2011.01.018.

[14] de Bresser J.H.P., J.H. ter Heege, and C.J. Spiers (2001). Grain size reduction by dynamic recrystallization: Can it result in major rheological weakening? Int. J. Earth Sci. 90, 28–45.

[15] Hirth, G., and D.L. Kohlstedt (2003). Rheology of the upper mantle and the mantle wedge: a view from the experimentalists. In: Eiler J. (Ed.), The Subduction Factory, Geophys. Monograph 138, 83– 105.

[16] Gueydan, F., J. Précigout, and L. Montési (2014). Strain weakening enables continental plate tectonics, Tectonophysics, in press, doi:10.1016/j.tecto/2014.02/005.

[17] Jackson, J. (2002). Strength of the continental lithosphere: time to abandon the jelly sandwich? GSA Today September, 1-9.

[18] Wray et al. (2013) Prolonged magmatic activity on Mars inferred from the detection of felsic rocks, Nature Geosci. 6, 1013-1017, doi: 10.1038/ngeo1994.

[19] Gueydan, F. et al. (2003). Analysis of continental midcrustal strain localization induced by microfracturing and reaction-softening, J. Geophys. Res. 108, 2064 doi:10.1029/2001JB000611.

Rheology of bubble- and crystal-bearing magma: new analogue experimental data and an effective-medium model

S. P. Mueller[1], J.M. Truby[2], E.W. Llewellin[2], H.M. Mader[3]

[1]*Institute of Geosciences, Johannes Gutenberg University Mainz, 55099 Mainz, Germany*
[2]*Department of Earth Sciences, Durham University, Durham DH1 3LE, UK*
[3]*School of Earth Sciences, University of Bristol, Bristol, BS8 2JJ, UK*
e-mail: *sebastian.mueller@uni-mainz.de*
session: *Rheology*

Introduction

Magma is a multiphase suspension: a complex mixture of a viscous silicate melt, a solid phase (crystals), and a gas phase (bubbles). The degree of interaction between bubbles and crystals, and the relative proportions of these phases, exert a major control on the bulk flow behaviour of the magma or lava. Characterizing, modelling, and predicting the flow of such a suspension requires a constitutive rheological model, encapsulating the viscosity of the suspension as a function of the properties of the suspending liquid and the volume fraction and properties of the suspended phase(s).

In contrast to two-phase mixtures (solid-liquid, gas-liquid), very little research has been directed at understanding the rheology of three-phase suspensions – primarily owing to the complexity of the problem – and no experimentally-validated constitutive rheological model has been published to-date. Constraining three-phase rheology therefore remains an important, yet outstanding, problem in geosciences, as well as in multiphase fluids research.

Here, we build on published two-phase constitutive equations to generate a three-phase model, by using an 'effective-medium' method in which the bubble suspension is treated as a continuous medium which suspends the particles. We validate the model against a set of new experimental data for three-phase suspensions of bubbles and spherical particles in the low capillarity regime (in which flow is steady and bubble deformation is small).

On the rheology of two-phase suspensions

Bubble suspensions

When a bubble suspension flows, viscous stresses cause the bubbles to deform. In a steady flow the bubbles reach an equilibrium deformation, which is described by the capillary number

$$Ca = \lambda\dot{\gamma} \tag{1}$$

where λ is the bubble relaxation time and $\dot{\gamma}$ the shear strain rate (Taylor 1934; Llewellin et al. 2002, Rust & Manga 2002). The relaxation time describes the characteristic timescale over which the bubble adjusts towards a new equilibrium deformation in response to a change in the strain environment, and depends on the liquid-gas interfacial tension Γ and the bubble radius a : $\lambda = \mu a/\Gamma$. For steady flow, the relative viscosity η_{r_b} of a bubble suspension is given by (Mader et al. 2013)

$$\eta_{r_b} \equiv \frac{\eta_b}{\mu} = \eta_{r,\infty} + \frac{\eta_{r,0} - \eta_{r,\infty}}{1 + (\frac{6}{5}Ca)^2} \tag{2}$$

where η_b is the viscosity of the bubble suspension, and $\eta_{r,0}$ and $\eta_{r,\infty}$ are, respectively, the relative viscosity of the bubble suspension at low and high Ca. For non-dilute suspensions, $\eta_{r,0}$ and $\eta_{r,\infty}$ are given by (Llewellin & Manga 2005; Mader et al. 2013)

$$\eta_{r,0} = (1 - \phi_b)^{-1} \tag{3}$$

and

$$\eta_{r,\infty} = (1 - \phi_b)^{5/2} \tag{4}$$

where ϕ_b is the bubble volume fraction.

Particle suspensions

Suspensions of solid particles are non-Newtonian (mostly shear-thinning) when non-dilute and their rheology is often described using a power law of the form

$$\eta_p = K\dot{\gamma}^{n-1} \tag{5}$$

where η_p is the apparent viscosity of the suspension, K is the consistency and n is the flow index which defines the degree of shear thinning. Mueller et al. (2011) demonstrate that the dependence of the relative consistency K_r on particle volume fraction ϕ_p is well described by the Maron-Pierce relationship (Maron & Pierce 1956)

$$K_r \equiv \frac{K}{\mu} = (1 - \frac{\phi_p}{\phi_m})^{-2} \tag{6}$$

where ϕ_m is the maximum packing fraction. The relative consistency is defined by analogy with the relative viscosity of the particle suspension $K_r \approx \eta_{r_p} \equiv \eta_p./\mu$. (Note that, strictly, the relative consistency is dimensionless only if $n = 1$, and is numerically equal to η_{r_p} only if $n = 1$ or $\dot{\gamma} = 1$. However, Mader et al. (2013) demonstrate that, in practice, K_r and η_{r_p} can be treated as equivalent for $10^{-3} \lesssim \dot{\gamma} \lesssim 10\ s^{-1}$ and $\phi_p/\phi_m \lesssim 0.5$).

The maximum packing fraction ϕ_m is a function of particle shape (i.e., particle aspect ratio, r_p) and roughness; Mader et al. (2013) give the following equation for rough particles (representative for crystals in magma):

$$\phi_m = 0.5\Big[- \frac{(log_{10} r_p)^2}{2}\Big] \tag{7}$$

A model for the rheology of three-phase suspensions

Equation (6) gives the consistency of a suspension of particles in a liquid with viscosity μ. If we suppose that the particles are instead suspended in a bubble suspension with viscosity η_b (i.e. we treat the bubble suspension as an 'effective medium') we obtain

$$\frac{K}{\eta_b} = \Big(1 - \frac{\phi_p}{\phi_m}\Big)^{-2} \tag{8}$$

At low Ca, from equations (2) and (3), we have $\eta_b = \mu(1 - \phi_b)^{-1}$, hence

$$K_r = (1 - \phi_b)^{-1}\Big(1 - \frac{\phi_p}{\phi_m}\Big)^{-2} \tag{9}$$

If, as in our model, the bubble suspension is treated as effective medium and continuous phase, particle and bubble volume fractions are commonly defined as

$$\phi_b = \frac{V_b}{V_l + V_b} \tag{10}$$

$$\phi_p = \frac{V_p}{V_l + V_b + V_p} \tag{11}$$

where V_l, V_b and V_p are the volumes of the liquid, bubble and particle phases, respectively.

For many three-phase applications, however, it makes more sense to consider the effect of *adding* bubbles to a particle suspension, rather than replacing liquid with gas. For example, a magma that contains solid crystals may be bubble-free at depth, but become increasingly bubble-rich during ascent. In this case, it is more intuitive to define a particle volume fraction and bubble volume fraction as follows:

$$\phi_b^* = \frac{V_b}{V_l + V_b + V_p} \tag{12}$$

$$\phi_p^* = \frac{V_p}{V_l + V_p} \tag{13}$$

In this formulation, the particle volume fraction does not change from its initial value as bubbles grow, and the bubble volume fraction reflects the value that would be measured using Archimedes' principle.

Analogue experiments

We performed a series of 42 rheology tests on three-phase analogue samples. The samples were prepared by adding spherical glass beads (Potters Ballotini; density 2448 kg/m^3, size fraction 63 to 125 μm) to a sugar syrup (Tate & Lyle Golden Syrup; density 1438 kg/m^3) and aerating with a domestic electric whisk. The rheology of the pure syrup was determined individually for each sample batch and found to be strictly Newtonian. Particle volume fraction was controlled by adding a known mass of beads to a known mass of syrup (typically equating to 100-150 ml) to prepare sample suites of similar initial (bubble-free) particle volume fraction ϕ_p = 0:05, 0.1, 0.2, 0.3, 0.4, and 0.5. Gas volume fraction was varied by adjusting the duration and speed of whisking, and suspension temperature. The bubble size distribution of each sample was determined using a sample image and the image analysis software JMicroVision.

Rheometric data were collected using a ThermoScientific Haake MARS II rheometer in concentric cylinder arrangement, at 20 °C. At steady flow experiments, a ramp of 20 incrementally increasing shear stresses (up to 500 Pa), and the corresponding strain rate values, is recorded - followed by a 20-step down-ramp. The consistency of each samples is determined by fitting the Herschel-Bulkley model to the corresponding τ vs $\dot{\gamma}$ flow curve (Figure 1, blue line):

$$\tau = \tau_0 + K\dot{\gamma}^n \qquad (14)$$

For some samples, the highest experimental strain rates are sufficient that the bubbles cannot be assumed to be in the low capillarity regime. We filter data to remove these datapoints by calculating a typical capillary number for each point. For this calculation, we assume the effective strain-rate in the bubbly effective medium to be approximately given by $\dot{\gamma}' = \dot{\gamma}/(1-\phi_p)$ (neglecting solid-body rotation of the particles). To determine a typical bubble radius for a sample, we calculate the volume-mean-radius $< a >= \Sigma a^4/\Sigma a^3$ where summation

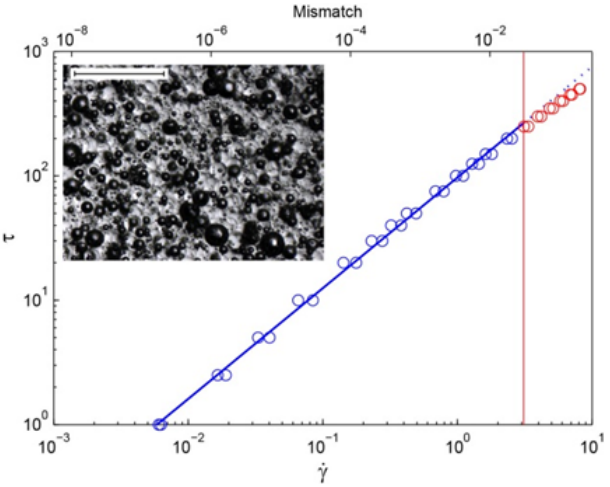

Fig. 1.: Exemplary flow curve of shear stress τ against strain rate $\dot{\gamma}$. Datapoints are collected during both the up-ramp and down-ramp, and fitted with the Herschel-Bulkley model (equation 14, blue line). Datapoints for which the deviation of the viscosity of the bubbly effective medium from the low capillarity assumption is greater than 5% are discarded (red line). Inset shows photomicrograph of a sample ($\phi_p = 0.42$; $\phi_b = 0.29$), in which dark-rimmed spheres are bubbles, and glass beads are light and translucent.

is over all measured bubbles in that sample (following Mader et al. 2013). Using $\dot{\gamma}$ and $< a >$ in equation (1) we obtain an effective capillary number Ca‘ for each datapoint, and a corresponding value of η_{r_b}. If the discrepancy between η_{r_b}b (which accounts for variable capillarity; eq. 2) and $\eta_{r,0}$ (which assumes $Ca \ll 1$; eq. 3) is greater than 5%, the datapoint is discarded (Figure 1, red line). After filtering, all flow curves comprise at least 14 datapoints.

Results

The resulting K_r values of 42 rheometric experiments on samples with 0 to 45 vol% particles and 0 to 28 vol% bubbles are displayed in Figure 2. From both Figure 2a and 2b, it becomes evident that the effect of adding bubbles a particle suspension depends upon the initial particle concentration ϕ_p^*. For dilute particle suspensions ($\phi_p^* \lesssim 0.25$), adding bubbles increases the bulk consistency, whereas for concentrated suspensions

with $\phi_p^* \gtrsim 0.25$ adding bubbles decreases bulk consistency.

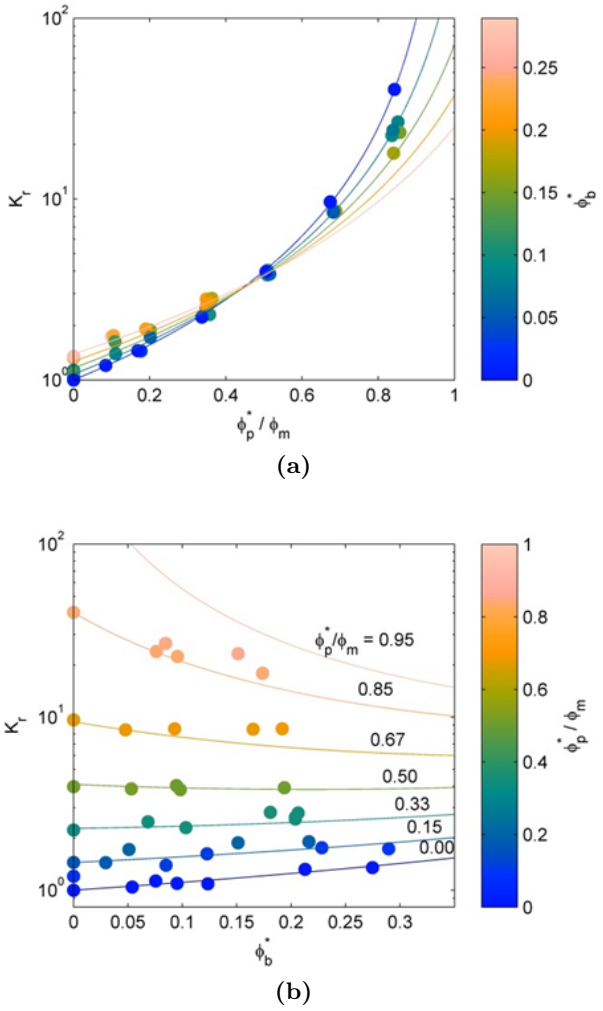

Fig. 2.: (a) Relative consistency K_r plotted against the particle concentration ϕ_p^* (normalized by the maximum packing fraction ϕ_m); circles are coloured according to ϕ_b^*. Solid lines are the three-phase model (equation 9). (b) K_r against gas volume fraction ϕ_b^*, with datapoints coloured according to ϕ_P^*. Again, solid lines are fits of equation 9.

The physical explanation for this behaviour is straightforward, and relies on two competing processes. The intrinsic effect of the addition of low capillarity (i.e. spherical) bubbles to a fluid is to increase its consistency. For dilute particle suspensions, this is the dominant trend, hence our data show an increase in consistency with increasing bubble content for $\phi_p^* \lesssim 0.25$. Opposing this is a 'dilution' process, in which the addition of bubbles to a suspension of particles moves the particles further apart; this decreases the particle volume fraction ϕ_p, reduces the impact that particle-particle interactions have on suspension rheology, and reduces suspension consistency. This process dominates for concentrated particle suspensions because the Maron-Pierce relationship is a power law; hence, the higher the initial particle volume fraction, the greater the impact the same dilution will have.

References

Llewellin, E. W., Mader, H. M. & Wilson, S. D. R. (2002) The rheology of a bubbly liquid. Proceedings of the Royal Society A: Mathematical, Physical and Engineering Sciences 458, 987-1016.

Llewellin, E. W. & Manga, M. (2005) Bubble suspension rheology and implications for conduit flow. Journal of Volcanology and Geothermal Research 143 (1-3), 205-217.

Mader, H. M., Llewellin, E. W. & Mueller, S. (2013) The Rheology of Two-Phase Magmas : A Review and Analysis. Journal of Volcanology and Geothermal Research 257, 1-51.

Maron, S. H. & Pierce, P. E. (1956) Application of Ree-Eyring generalized flow theory to suspensions of spherical particles. Journal of Colloid Science 11, 80-95.

Mueller, S., Llewellin, E. W. & Mader, H. M.(2011) The effect of particle shape on suspension viscosity and implications for magmatic flows. Geophysical Research Letters 38.

Rust, A. C. & Manga, M. (2002) Effects of bubble deformation on the viscosity of dilute suspensions. Journal of Non-Newtonian Fluid Mechanics 104, 53-63.

Taylor, G. I. (1934) The formation of emulsions in definable fields of flow. Proceedings of the Royal Society A: Mathematical, Physical and Engineering Sciences 146, 501-523.

Modeling stress evolution around a rising salt diapir

Maria A. Nikolinakou[1], Peter B. Flemings[1], Michael R. Hudec[1]

[1] *Bureau of Economic Geology, The University of Texas at Austin*
e-mail: *mariakat@mail.utexas.edu*
session: *Rheology*

Overview

We simulate the evolution of a salt diapir during sedimentation and study how deposition and salt movement affect stresses close to the diapir (Figure 1). We model the wall rocks as porous elastoplastic materials. Our analysis shows that stresses rotate near a salt diapir, such that the maximum principal stress is perpendicular to the contact with the salt. The minimum principal stress is in the hoop direction, and drops near the salt, resulting in a reduced range of acceptable drilling mud weights. The mean stress increases near the upper parts of the diapir, leading to a porosity that is lower than predicted for uniaxial burial at the same depth.

Because we simulate sedimentation simultaneously with the movement of the salt, our study offers two major achievements distinct from previous work on salt-diapir and sediment interaction: the salt is not kinematically prescribed and the stresses within the basin develop as a function of both the depositional process and the loading from the salt. Consequently, the porosity-depth profile in our model differs from that of a basin that has been uniaxially deposited; here, the wall rocks are denser near the growing dome.

Finite-element model

We built our numerical model within the finite-element program Elfen®(Peric and Crook, 2004, Rockfield, 2010, Thornton et al., 2011). We study the evolution of a three-dimensional salt diapir using an axisymmetric model (360° rotation of the vertical section shown in Figure 2). There is no slip between the diapir and the basin. The base and side boundaries are rollers (zero-normal-displacement, free-slip boundaries), and the model is wide enough that the side boundary is unaffected by any stress perturbations. The initial stresses in the model are geostatic (K_0=0.8). Pore pressures are assumed hydrostatic and do not change during the analysis (drained simulation). We simulate sedimentation by aggrading the top of the model 400 m every half million years.

We model the salt as a solid viscoplastic material with an equivalent salt viscosity between $10^{18} - 10^{20}$ Pas, using a reduced form of the Munson and Dawson formulation (Munson and Dawson, 1979). Basin sediments are modeled as porous elastoplastic, using the SR3 constitutive model, which is based on the principles of Modified Cam Clay (Muir Wood, 1990, Rockfield, 2010)

Stresses within the wall rocks

Rise of a salt diapir loads the wall rocks, because the salt expands out as it moves up. In the circumferential (hoop) direction, the diapir radius increases, leading to significant extensional hoop strains; as a result, the hoop (or circumferential) stress decreases in comparison to the far-field horizontal/hoop stress (Figure 3b). On the other hand, as the salt diapir is pushing outwards, it radially compresses the sediments (Figure 3a). This increases the horizontal stress (green solid line in Figure 3b) above its far-field value (dotted gray line) and to values even higher than the integration of the overburden (dashed gray line)

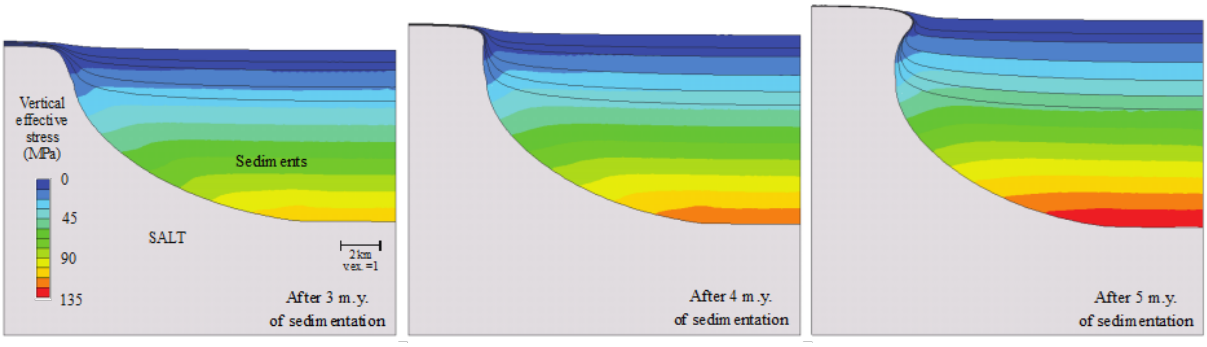

Fig. 1.: Vertical sections predicted by the numerical model after 3, 4, and 5 m.y. of sedimentation. Contours illustrate changes in vertical stress due to sedimentation and simultaneous salt movement (Nikolinakou et al., 2014).

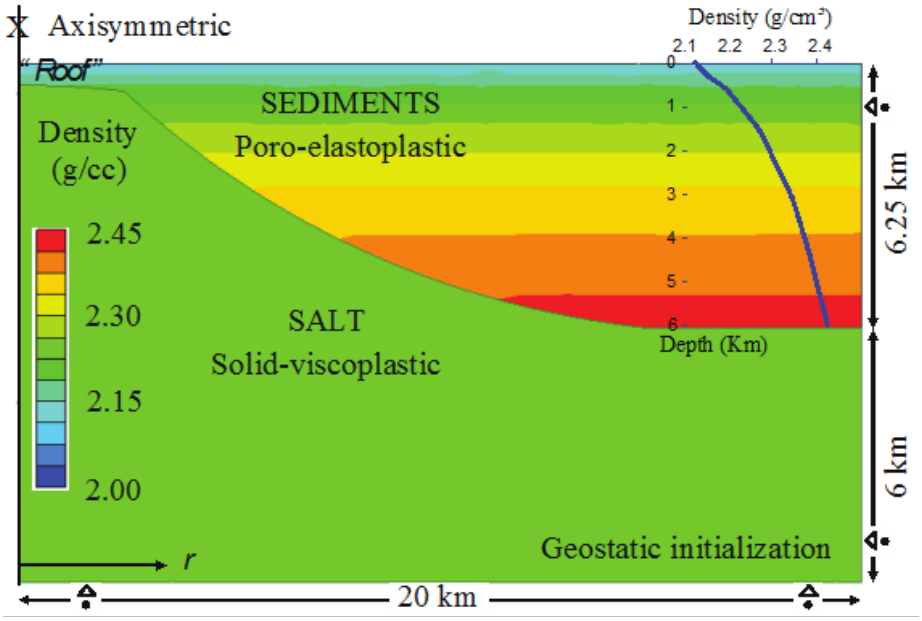

Fig. 2.: Plane of revolution for axisymmetric numerical model (vertical section). Contours and inset plot show density-depth profile of initial section (Nikolinakou et al., 2014).

close to the upper parts of the diapir. The vertical stress (dotted solid purple line in Figure 3b) decreases in the sediments next to the salt diapir. This decrease is associated with a rotation of the principal stresses near the salt-sediment interface. The maximum principal stress (σ_1) becomes perpendicular to the salt face and increases to a value equal to the stress inside the salt. Near the dome, the minimum principal stress is in the circumferential (hoop) direction, because of the circumferential expansion of the diapir during its rise.

The combination of the stress changes near the salt (Figure 3) leads to a net increase of the mean stress close to the upper parts of the diapir, and a decrease near the base of the diapir, compared to the far-field values at the same depth (Figure 4a). Consequently, the porosity near the vertical parts of the salt diapir is lower than the porosity predicted by a uniaxial compression model (Figure 4b), as the sediments have been locally compressed to a higher stress level.

Discussion

Our results show that near a rising salt diapir, the minimum principal stress is in the circumferential (hoop) direction. This suggests that radial normal faults should be favored near the diapir, as is commonly observed (Davison et al., 2000, O'Brien and Lerch, 1987, Stewart, 2006). The predicted decrease in the hoop stress also means that the fracture gradient is reduced near the salt; in practice, this suggests a narrower range of admissible drilling mud weights. Indeed, reduced stress values at the circumferential (hoop) direction are often reported near salt diapirs and such stresses are associated with borehole instabilities and loss of circulation (Bradley, 1978, Seymour et al., 1993, Dusseault et al., 2004). Furthermore, our model predicts a higher mean stress near the upper parts of the diapir; indeed, denser sediments have been observed near the "shoulders" of salt diapirs in the North Sea (Dusseault et al., 2004)

Such comparisons illustrate that evolutionary models can provide a detailed understanding of the stress history of mudrocks close to salt diapirs and hence improve predictions of stresses, possible fault directions, shear/tensile strength, and material properties of the wall rocks.

References

Bradley, W. B., 1978, Borehole failure near salt domes: Society of Petroleum Engineers Annual Fall Technical Conference and Exhibition, 10/01/1978, at Houston, Texas

Davison, I., I. Alsop, P. Birch, C. Elders, N. Evans, H. Nicholson, P. Rorison, D. Wade, J. Woodward, and M. Young, 2000, Geometry and late-stage structural evolution of Central Graben salt diapirs, North Sea: Marine and Petroleum Geology, 17, no. 4, 499-522. doi: http://dx.doi.org/10.1016/S0264-8172(99)00068-9.

Dusseault, M. B., V. Maury, F. Sanfilippo, and F. J. Santarelli, 2004, Drilling Around Salt: Risks, Stresses, And Uncertainties, 5-9 June 2004 Muir Wood, D., 1990, Soil behaviour and critical state soil mechanics: Cambridge University Press.

Munson, D. E., and P. R. Dawson, 1979, Constitutive model for the low temperature creep of salt (with application to WIPP), in SAND79-1853Sandia National Laboratories, Albuquerque, NM

Nikolinakou, M. A., P. B. Flemings, and M. R. Hudec, 2014, Modeling stress evolution around a rising salt diapir: Marine and Petroleum Geology, 51, 230-238. doi: http://dx.doi.org/10.1016/j.marpetgeo.2013.11.021.

O'Brien, J. J., and I. Lerch. 1987, Modellingof the deformation and faulting of theformations overlying an uprising saltdome., in I. Lerche and J. J. O'Brien, eds., Dynamical Geology of Saltand Related Structures: Academic Press, London. 419–455.

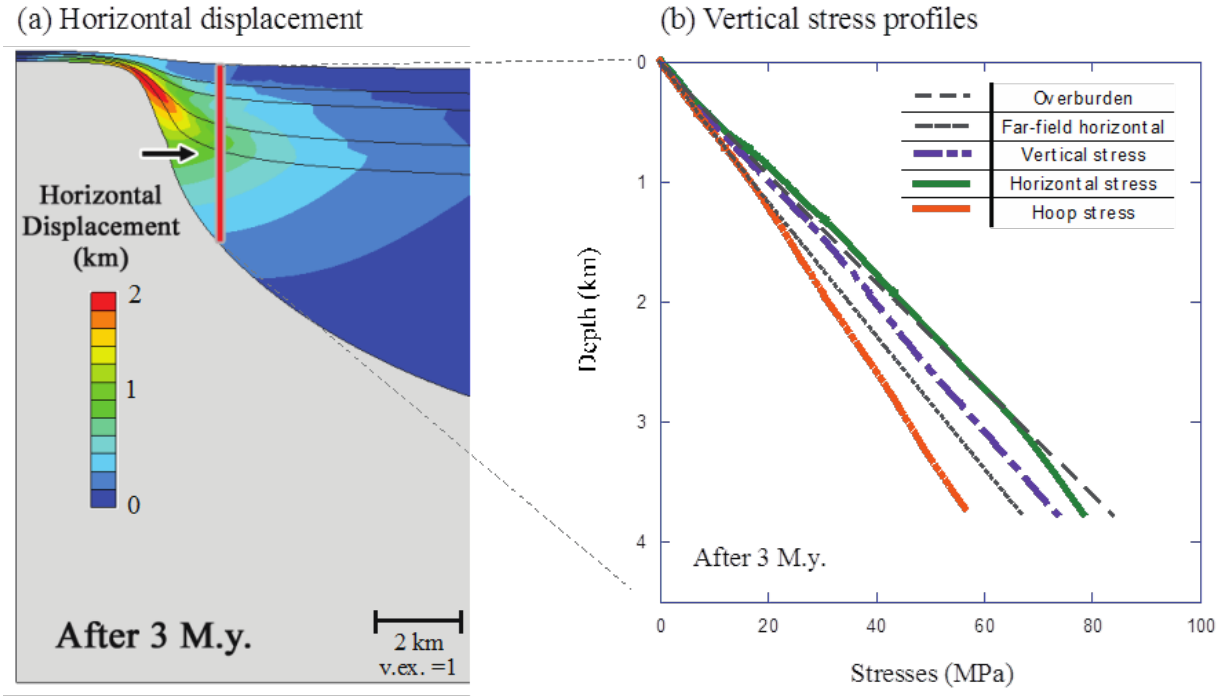

Fig. 3.: (a) Vertical section with contours of horizontal displacement next to rising salt dome, after 3 m.y. of deposition; (b) Stress profiles of horizontal, vertical, and hoop stresses along well next to salt. (Nikolinakou et al., 2014).

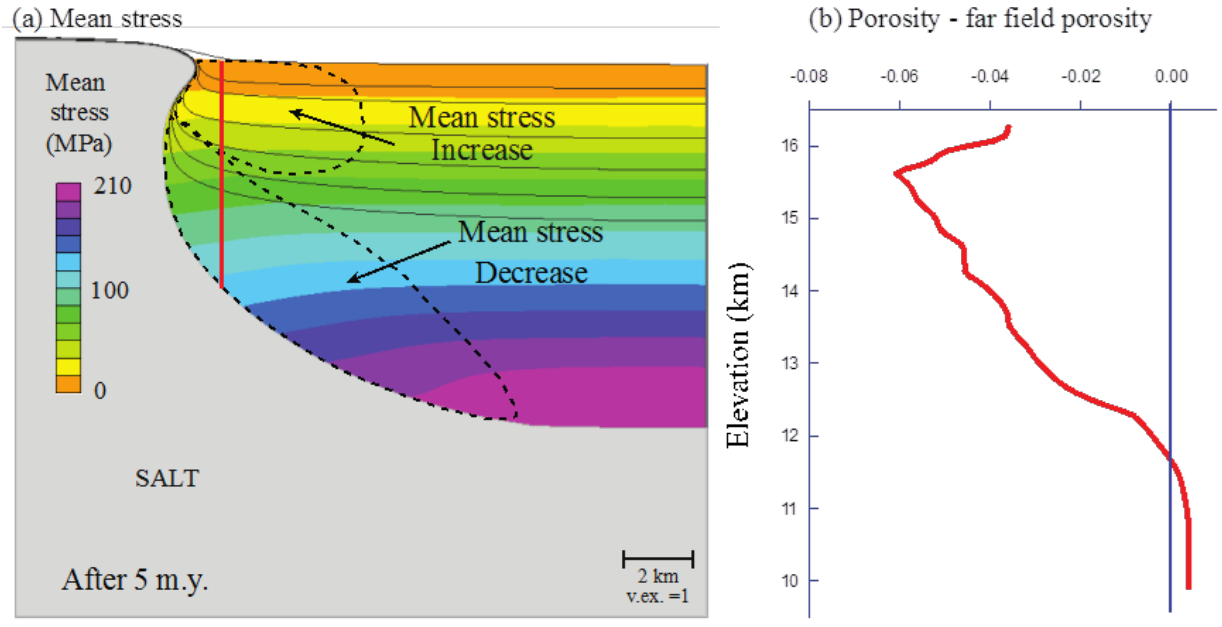

Fig. 4.: (a) Vertical section showing mean stress contours near rising salt dome after 5 m.y. of deposition; b) profile along vertical well plotting difference between measured and far-field porosity (Nikolinakou et al., 2014).

Peric, D., and A. J. L. Crook, 2004, Computational strategies for predictive geology with reference to salt tectonics: Computer Methods in Applied Mechanics and Engineering, 193, no. 48,Äì51, 5195-5222. doi: http://dx.doi.org/10.1016/j.cma.2004.01.037.

Seymour, K. P., G. Rae, J. M. Peden, and K. Ormston, 1993, Drilling close to salt diapirs in the North Sea: Offshore Europe, 09/07/1993, at Aberdeen, U.K.

Stewart, S. A., 2006, Implications of passive salt diapir kinematics for reservoir segmentation by radial and concentric faults: Marine and Petroleum Geology, 23, no. 8, 843-853. doi: http://dx.doi.org/10.1016/j.marpetgeo.2006.04.001.

Thornton, D. A., D. T. Roberts, A. J. L. Crook, and J. G. Yu, 2011, Regional scale salt tectonics modelling: Bench-scale validation and extension to field-scale propblems.: Beyond balanced sections: Geological Society of America Conference, at Minneapolis, USA.

Numerical bifurcation analysis of spontaneous strain localization resulting in necking of a layer

M. Peters[1], T. Poulet[2], M. Veveakis[2], A. Karrech[3], M. Herwegh[1], K. Regenauer-Lieb[2,4]

[1]*Institute of Geological Sciences, University of Bern, Switzerland*
[2]*CSIRO Earth Science and Resource Engineering, Kensington, Western Australia*
[3]*School of Civil and Resource Engineering, The University of Western Australia*
[4]*School of Earth and Environment, The University of Western Australia*
e-mail: *max.peters@geo.unibe.ch*
session: *Rheology*

Introduction

During necking of a mechanically stiff layer embedded in a weaker matrix, relatively large amounts of strain localize in small areas. As this deformation style appears under distinct geological conditions, necking phenomena, e.g. *boudinaged* mineral veins, are associated with a variety of deformation modes. These modes have been identified and recently numerically modeled as extensional fracturing (Abe and Urai, 2012), bookshelf-gliding or pinch-and-swell structures (Schmalholz and Maeder, 2012). In the latter case, i.e. *continuous necking*, symmetric boudins are interpreted as the result of dominant viscoplastic deformation (Goscombe et al., 2004). This study focuses on such deformation structures and the origin of the instabilities provoking necking. Indeed the driving mechanisms are currently not very well understood. In this light, we will explore their role as precursory structures, i.e. storage and potential localization of elastic energy affecting further plastic deformation (e.g. Regenauer-Lieb & Yuen, 1998; 2004; Karrech et al., 2011a) and the flow regime during localization. With this respect coupling of state, rheology and thermal-mechanics was chosen.

Method

In this work we have implemented the coupled model, recently presented by Herwegh et al. 2014, comprising multiple rheologies (elastic, rate-independent plasticity, diffusion creep, dislocation creep) and accounting for grain size variations. The resulting system of equations was solved in a shear box setting, for constant velocity conditions with a finite element solver (Karrech et al, 2011a). We simulate a pure-shear box with constant velocity boundary condition, using finite elements of which each element represents a grain size distribution. The box is built up by 3 layers, consisting of a central layer of coarse-grained populations that are allowed to evolve with time, surrounded by finer-grained populations with fixed grain sizes. The rheology of the central layer evolves from transient stages (linear elasticity and strain hardening) to composite viscous flow (dislocation + diffusion creep) with increasing shear strain. The small grain sizes in top and bottom layers are strain-invariant and limited in their growth (comparable to *Zener pinning* in nature) forcing the matrix to exclusively deform by diffusion creep. In contrast, the initially coarse-grained central layer is allowed to adapt to the physical deformation conditions by either grain growth (subscript g) or grain size reduction (subscript r) following the *Paleowattmeter* of Austin and Evans (2007; 2009):

$$d_s = k' \sigma^{-m'} exp\Big(\frac{-Q'}{RT}\Big)$$

where

$$k' = \Big[\frac{c\gamma A_g}{\lambda P A_{dis}}\Big]^{1/(p+1)}$$

$$m' = \frac{n+1}{p+1}$$

$$Q' = \frac{Q_g - Q_r}{p+1}$$

where d_s is the steady-state grain size, σ the flow stress, Q the activation enthalpy, R the gas constant, T the absolute temperature, c a geometric constant (π for spherical grains), γ the grain boundary energy, A the pre-exponential factor of the corresponding power-law creep behavior, λ the energy fraction deposited in the microstructure, p the grain growth exponent and n the stress exponent.

We embedded the grain size evolution in the thermodynamic approach of Regenauer-Lieb and Yuen (2004) and expended it to the transient regime. The total energy budget reads:

$$\underbrace{\rho c_p \frac{dT}{dt}}_{\text{energy budget}} = \underbrace{\chi\left(\sigma_{ij}\dot{\varepsilon}_{ij} - \rho\frac{\partial\psi}{\partial\varepsilon_{ij}^{el}}\dot{\varepsilon}_{ij}^{el} - \rho\frac{\partial\psi}{\partial d}\dot{d}\right)}_{\text{dissipative work}} + \underbrace{\rho T\frac{\partial^2\psi}{\partial\varepsilon_{ij}^{el}\partial T}\dot{\varepsilon}_{ij}^{el}}_{\text{thermal-elastic heat}} + \underbrace{\rho T\frac{\partial^2\psi}{\partial d\partial T}\dot{d}}_{\text{grain size heat}} + \underbrace{\kappa\nabla^2 T}_{\text{heat conduction}}$$

where ρ is the mass density, c_p the specific heat, χ the Taylor-Quinney coefficient ($\chi = 1 - \lambda$), ϵ the elastic strain, d the mean grain size, ψ the Helmholtz free energy and κ the thermal conductivity. For a detailed description of the modeling technique the reader is referred to Herwegh et al. (2014).

In addition, linear perturbation analyses were performed in order to evaluate the imperfection sensitivity in the elastic (and viscous) regimes. We perform a classical modal analysis to determine the natural mode shapes and frequencies of the geological structure during arbitrarily imposed vibrations. This analysis aims at detecting the *eigenmodes* of the system, which are sinusoidal vibrations with geometry specific modal shapes and frequencies. The *eigenvalues* represent the nodal points where the onset of (visco)-elasto-plastic localization can initiate in the structure (Rice, 1976). The *eigenmodes*, *eigenvalues* and *eigenvectors* are highly sensitive to the layer-box aspect ratio and material properties, i.e. differences in Young's moduli, or effective viscosity, respectively. These preloading structures were then used as seeds for imperfections in the succeeding modeling of boudinage in order to overcome instabilities that may arise from geometry and to reduce computational time. Moreover, further sensitivity studies were performed in order to exclude boundary effects, such as mesh or rheological parameter sensitivities or perturbations from numerical noise.

Results

Bifurcation from homogeneous state

With increasing extensional strain, grain sizes converge to a steady state, i.e. viscous relaxation of the calcite (Fig. 1). It becomes obvious that localization then occurs from steady state. The total energy budget thus reduces to the terms of dissipative work and heat conduction. By means of an instability analysis, first described by Gruntfest (1963), we can uncover the time-independent critical threshold for which localization will occur in terms of the ratio of mechanical energy, which is converted into heat, over the diffusive capacity of the system, also known as the *Gruntfest number*, or critical dissipation, in dependence of the layer dimension l_y:

$$Gr = \chi\frac{A_{dis}l_y^2}{\kappa T_{boundary}}\sigma^{n,disl}exp\Big(\frac{-Q_{disl}}{RT_{boundary}}\Big)$$

Post-localization viscous creep

Depending on the dissipated energy, grain sizes in the modeled domains vary substantially in space and time. While low stresses in the swells favor grain growth and diffusion creep, high stresses in the pinches provoke dramatic grain size reduction with an increasing contribution of dislocation creep. The development of symmetric necks thus seems to coincide with the transition from dislocation to diffusion creep dominated flow with continuous grain size reduction in the necks and growth in the swells, respectively. Linked with the grain size reduction is strain localization within the necks at relatively low extensional strains.

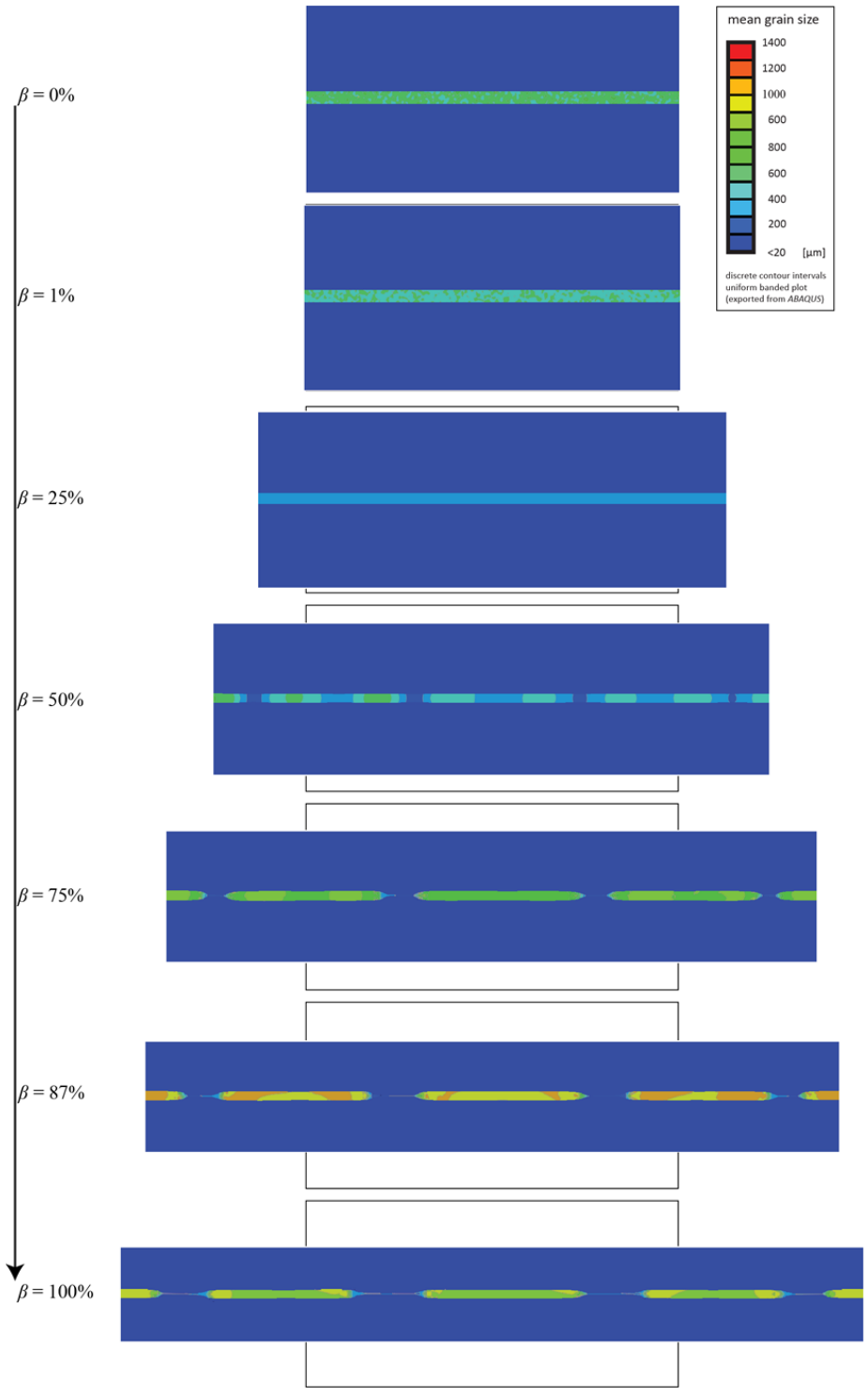

Fig. 1.: Numerical simulation of a coarse-grained ($500\mu m \pm 2\sigma$) calcite layer embedded in a finer-grained ($10\mu m \pm 2\sigma$) calcitic matrix. Boundary conditions: Strain rate=1.0E-14 $^{s-1}$, Temperature=300°C. β=relative extensional strain.

Concluding remarks

The focus of our ongoing work is to understand necking phenomena and the comparison between numerical simulations and natural microstructures. We have shown that visco-plastic necking of a numerical calcite layer occurs for natural deformation conditions and deformation mechanisms from *steady-state* composite viscous creep. The difference in effective viscosity between layer and matrix is around 1 order of magnitude, which underlines the contribution of an additional weakening effect, i.e. shear heating. Moreover, the thermo-dynamic feedbacks allow microstructural work, acting as an energy sink, which limits the actual contribution of shear heating to less than 2 K. Nevertheless, an instability study (Gruntfest, 1963) reveals the amount of critical dissipation necessary to trigger a perturbation resulting in localization.

Furthermore, we reveal that elastic stress concentrations control localized visco-plastic deformation, which is expressed by plastic strain energy increase in necking structures, as previously discussed by Regenauer-Lieb and Yuen (2004). This finding underlines the importance of the *transient* deformation regime as trigger for plastic deformation and the need for thermodynamics-based (total) energy considerations. Finally, we will discuss the effects of perturbations, which seem to be a prerequisite for solely mechanics-based simulations in which localization is driven by geometry, compared to our case, in which the microphysical deformation behavior of the system drives strain localization.

References

Abe, S. and Urai, J.L. (2012). Discrete element modeling of boudinage: insights on rock rheology, matrix flow, and evolution of geometry. Journal of Geophysical Research, 117.

Austin, N. and Evans, B. (2007). Paleowattmeters: A scaling relation for dynamically recrystallized grain size. Geology, 35.

Austin, N. and Evans, B. (2009). The kinetics of microstructural evolution during deformation of calcite. Journal of Geophysical Research, 114.

Goscombe, B.D., Passchier, C.W. and Hand, M. (2004). Boudinage classification: End-member boudin types and modified boudin structures, Journal of Structural Geology, 26.

Gruntfest, I.J. (1963). Thermal feedback in liquid flow; plane shear at constant stress. Transactions of the Society of Rheology, 7.

Herwegh, M., Poulet, T., Karrech, A. and Regenauer-Lieb, K. (2014). From transient to steady state deformation and grain size: A thermodynamic approach using elasto-visco-plastic numerical modeling, J. Geophys. Res. Solid Earth, 119.

Karrech, A., Regenauer-Lieb, K. and Poulet, T. (2011a). A Damaged visco-plasticity model for pressure and temperature sensitive geomaterials. Journal of Engineering Science, 49.

Regenauer-Lieb, K., Yuen, D. (1998). Rapid conversion of elastic energy into plastic shear heating during incipient necking of the lithosphere. Geophysical Research Letters, 25.

Regenauer-Lieb, K., Yuen, D. (2004). Positive feedback of interacting ductile faults from coupling of equation* of state, rheology and thermal-mechanics. Physics of the Earth and Planetary Interiors, 142.

Rice, J. R. (1976). The localization of plastic deformation. Theoretical and Applied Mechanics, 1.

Schmalholz, S.M. and Maeder, X. (2012). Pinch-and-swell structure and shear zones in visco-plastic layers. Journal of Structural Geology, 37.

Finite element model investigation of fault shear stress accumulation due to elastic loading and viscous relaxation.

Hiroki Sone[1]

[1] *German Research Centre for Geosciences, Potsdam, Germany*
e-mail: *sone@gfz-potsdam.de*
session: *Rheology*

Recent seismological observations from megathrust earthquakes in subduction zones (e.g. Sumatra, Maule, Tohoku) show that sources of relatively high and low frequency seismic waves are not necessarily co-located along a ruptured fault plane. As frequency of seismic waves reflect the rupture style which is influenced by preexisting shear stresses on the fault, some authors have accordingly suggested that the nature of the spatial stress heterogeneity along the subduction zone is depth dependent (Lay et al., 2012). However, we have little specific understanding about how such stress heterogeneities arise along fault planes, how they evolve throughout an earthquake cycle, or how it is affected by depth-dependent rheology. It is important to understand these interseismic processes because the initial stress condition prior to an earthquake has first order controls on how large an earthquake grows.

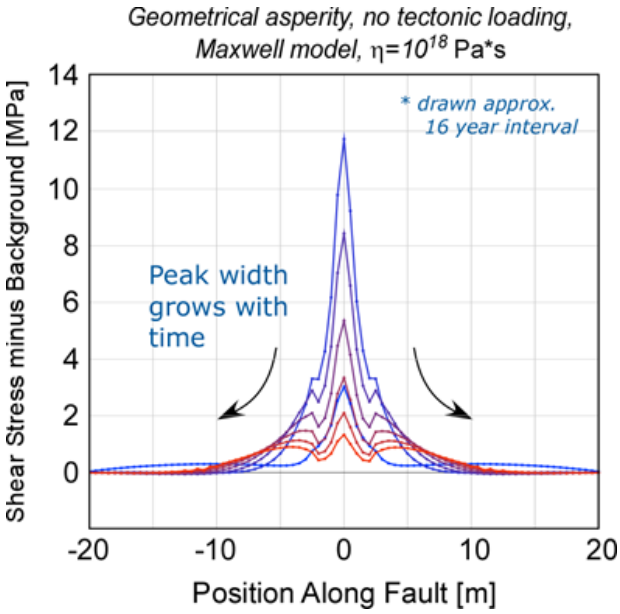

Fig. 1.: Relaxation of a stress concentration due to a geometrical asperity on the fault plane. The shear stress profile relative to the background level is drawn against the position along the fault plane. The profile evolves from blue to red, describing the growth in length scale of the stress concentration.

The focus of this study is to explore how stress concentrations on faults behave between earthquakes under some assumptions about the fault zone and host rock rheology. A generic fault zone model in a finite element code is used to investigate how the accumulation of shear stress along faults are influenced by the type of asperity (geometrical vs. stress), interseismic loading rate, and the mechanical properties of the fault zone and host rock materials. Fault stress accumulation is usually modeled by considering a frictionally locked fault interface embedded in an elastic lithosphere. However, many rocks exhibit viscoelastic behavior over geological time scales, especially true for fault related rocks which can be clay-rich and in-cohesive relative to the surrounding rocks. Thus particular emphasis of this study is to use viscoelastic rheology for the fault zone material to account for not only the elastic tectonic loading on faults, but also the viscous relaxation of stress over time.

Results of the modeling suggest that spatial diffusion of stress heterogeneities can occur due to viscoelastic effects especially when geometrical complexity is introduced at the fault surface.

(Figure 1) That is, the length scale of the stress concentration can grow over time as viscous deformation takes place in the viscoelastic fault zone. It is also found that the time scale required for the spatial diffusion of stress is influenced by the effective viscosity of the fault zone. This suggests that rheological properties can influence the size of stress patches, or "asperities", that can develop along a fault over a certain interseismic loading period. Comparison of results between different viscoelastic rheology and different tectonic loading rates will also be investigated to identify the relevance to natural settings.

References

Lay, T., Kanamori, H., Ammon, C.J., Koper, K.D., Hutko, A.R., Ye, L., Yue, H., and Rushing, T.M., Depth-varying rupture properties of subduction zone megathrust faults. Journal of Geophysical Research, 117, B04311, doi:10.1029/2011JB009133, 2012.

Lithospheric strength and elastic thickness variations in the North American continent

Magdala Tesauro[1,2], Mikhail K. Kaban[2], Sierd Cloetingh[1], Walter D. Mooney[3]

[1] *Department of Earth Sciences, Utrecht University, The Netherlands*
[2] *German Research Center for Geosciences (GFZ), Potsdam, Germany*
[3] *USGS, Menlo Park, USA*
e-mail: *magdala@gfz-potsdam.de*
session: *Rheology*

We estimate the strength and effective elastic thickness (*Te*) of the North American (NA) lithosphere (Tesauro et al., 2014a). To this purpose, we use two thermal models, which are corrected for compositional variations and anelasticity effect in the upper mantle (Figs. 1a-b), obtained in a joint inversion of the gravity data and two recent seismic tomography models NA07 (Bedle and van der Lee, 2009) and SL2013sv (Shaffer and Lebedev, 2013).

The method implies the construction of a preliminary 3D density model (Kaban et al., 2014), reflecting the effect of both thermal and compositional variations of the upper mantle. Such a model was obtained from a joint inversion of the residual mantle gravity anomalies, estimated by subtracting the gravity effect of the crust from the observed gravity field, and the residual topography. Afterwards, the two tomographic models were inverted for temperature using mineral physics equations (e.g., Stixrude and Lithgow-Bertelloni, 2005). In the initial inversion a uniform fertile composition was used. The initial thermal models made it possible to separate the effect of temperature and composition in the mantle residual gravity anomalies (Kaban et al., 2014). These preliminary results are obviously biased by not considering composition variations in the constructed thermal model (e.g., Griffin et al., 2003). To overcome this problem the initial compositional density anomalies under the cratons are interpreted in terms of degree of depletion in heavy constituents (CPX, garnet and *Fe*), and thus the thermal model is re-estimated, using the new composition (Tesauro et al., 2014b). These steps are repeated until the convergence is reached.

The crustal rheology is assigned using NACr14 (Tesauro et al., 2014c), the most recent NA crustal model, providing velocity and thickness for the three layer model of the crystalline crust. According to NACr14, we assign a 'hard' rheology (Type 5, Fig.2) represented by granite-diabase-mafic granulite to the regions characterized by high crustal velocities (e.g., the northern Rocky Mountains) and a 'soft' rheology (Type 1, Fig.2), represented by quartzite-diorite to regions with low crustal velocities (e.g., the continental margins). Between these two end-members we define several other rheologies given by a combination of these lithotypes, assigned to the areas with intermediate crustal velocities (Fig. 2).

The obtained strength models (Figs. 3-ab), identified with the same names as of the tomography models, evidence a sharp contrast between the weak off-cratonic regions, where the strength is prevalently localized in the crust, and the inner part of the cratons, characterized by strong lithosphere. Such a difference has been already observed in global strength models (e.g., Tesauro et al., 2012), but differently from previous results, the new models show that the Phanerozoic structures close to the edge of the cratons, as the Appalachians, are characterized by low strength,

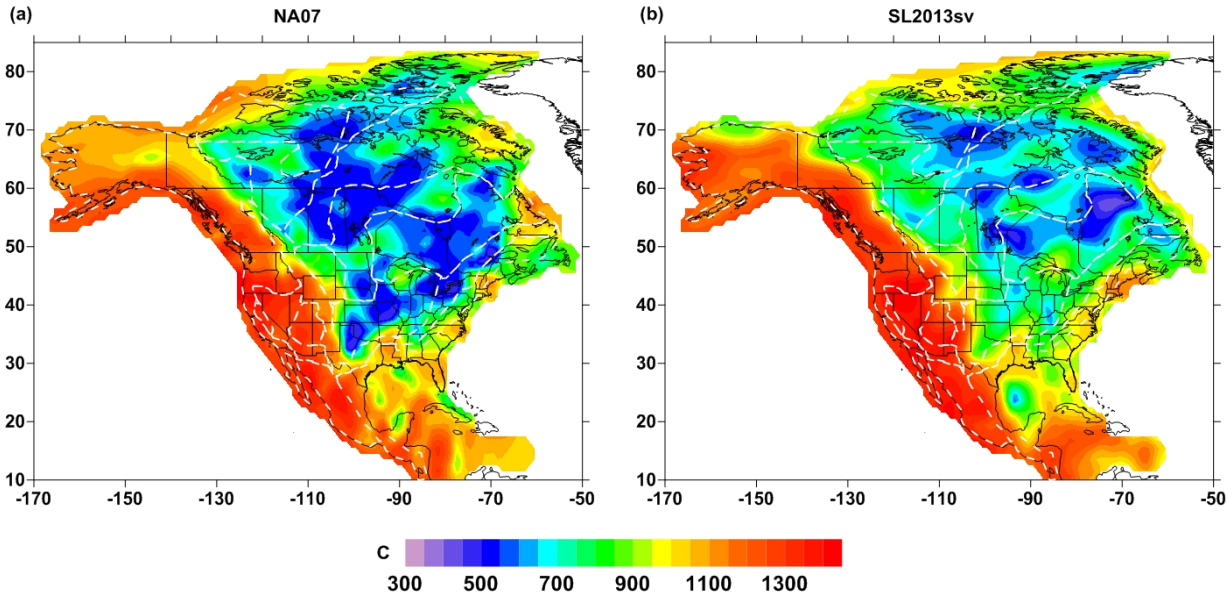

Fig. 1.: Temperature variations in the upper mantle (C°), 100 km depth (Tesauro et al., 2014b), estimated from joint inversion of the gravity and tomography data. Two tomography models have been employed: (left) the regional tomography model NA07 and (right) the global tomography model SL2013sv. White dashed contours as in Figs. 2-4 show the boundaries between tectonic provinces.

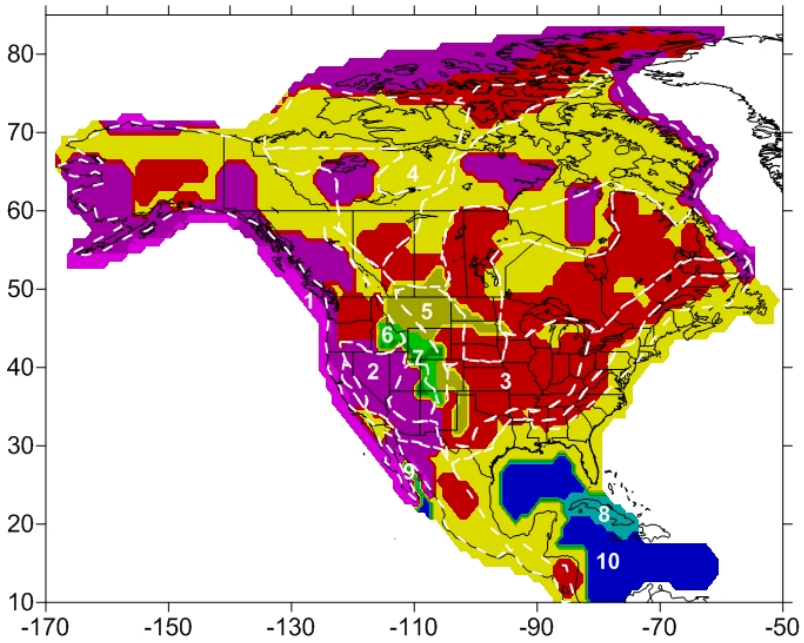

Fig. 2.: Rheological types of the crustal layers (Tesauro et al., 2014a), assigned on the base of the crustal velocity variations in NACr14 (Tesauro et al., 2014c), are identified by colours and white numbers, as follows: 1, Dry Quartzite-Wet Diorite-Wet Diorite; 2, Dry Quartzite-Wet Diorite-Dry Diabase; 3, Dry Granite-Wet Diorite-Mafic Granulite; 4, Dry Granite-Wet Diorite-Dry Diabase; 5, Dry Granite-Dry Diabase-Mafic Granulite; 6, Dry Quartzite-Dry Diabase-Dry Diabase; 7, Dry Quartzite-Wet Diorite-Mafic Granulite; 8, Dry Granite-Mafic Granulite; 9, Wet Quartzite-Wet Diorite; 10, Diabase.

while zones of local weakness are also present within the cratons. NA07 and SL2013sv differ chiefly in some peripheral parts of the cratons, as the Proterozoic Canadian Platform, the Grenville and the western part of the Yavapai-Mazatzal province, where the integrated strength in NA07 is ten times larger than in SL2013sv, reflecting the difference in the uppermost mantle temperatures (>200°C).

In terms of *Te* (Figs. 4a-b) estimated from the strength distribution the differences between the two models are less pronounced. In both of them only the most peripheral parts of the cratons, comprising Proterozoic regions reactivated by Meso-Cenozoic tectonics (e.g., Rocky Mountains and the Mississippi Embayment), are weak due to the absence of a mechanically strong part of the mantle lithosphere and thus more prone to instability. Intraplate earthquakes are distributed along the edges of the cratons, demonstrating that tectonic stress accumulates there more easily, while the core of the cratons remains undeformed. In both models half or more of these events occur in the weak lithosphere with the values of the integrated strength and *Te*, limited to a small range ($\sim 0.5 \times 10^{13}$ Pa s and ∼15 km, respectively), while the remaining part is located in the lithosphere characterized by pronounced contrast of strength and *Te*.

References

Bedle, H., van der Lee, S., 2009. S velocity variations beneath North America. J. Geophys. Res., 114, B07308, doi:10.1029/2008JB005949.

Griffin, W.L., O'Reilly, S.Y., Abe, N., Aulback, S., Davies, R.M., Pearson, N.J., Doyle, B.J., Kivi, K., 2003. The origin and evolution of Archean lithospheric mantle. Precambrian Res., 127, 19–41.

Kaban, M.K., M., Tesauro, M., Mooney, W.D., Cloetingh, S.A.P.L., 2014. Density, temperature and composition of the North American lithosphere: new insights form a joint analysis of seismic, gravity and mineral physics data. Part I: Density structure of the crust and upper mantle. Geophys. Geochem. Geosyst. (submitted).

Schaeffer, A.J., Lebedev S., 2013. Global shear-speed structure of the upper mantle and transition zone. Geophys. J. Int., 194, (1), 417-449.

Schulte, S., Mooney, W.D., 2005. An updated global earthquake catalogue for stable continental regions: reassessing the correlation with ancient rifts. Geophys. J. Int. 161, 707–721.

Stixrude, L., Lithgow-Bertelloni, C., 2005. Thermodynamics of mantle minerals – I. Physical properties. Geophys. J. Int., 162, 610–632.

Tesauro, M., Kaban, M.K., Cloetingh, S.A.P.L., 2012a. Global strength and elastic thickness of the lithosphere. Global and Planetary Change 90–91, 51–57.

Tesauro, M., Kaban, M., Mooney, W.D., Cloetingh, S.A.P.L., 2014a. Lithospheric strength and elastic thickness variations in the North American continent. Earth and Planetary Science Letters (submitted).

Tesauro, M., Kaban, M., Mooney, W.D., Cloetingh, S.A.P.L., 2014b. Density, temperature and composition of the North American lithosphere: new insights form a joint analysis of seismic, gravity and mineral physics data. Part II: Thermal and compositional model of the upper mantle. Geophys. Geochem. Geosyst. (submitted).

Tesauro, M., Kaban, M., Mooney., W.D., Cloetingh, S.A.P.L., 2014c. A 3D model for the crustal structure of the North American Continent. Tectonophysics, in press.

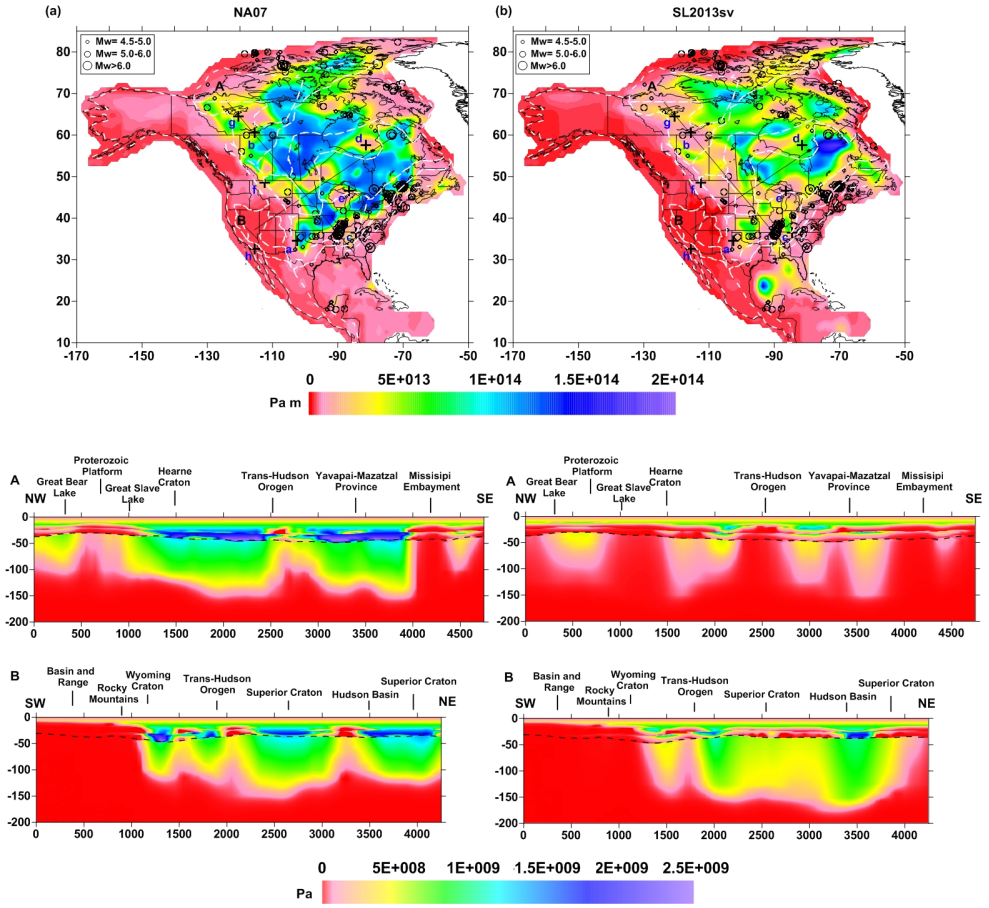

Fig. 3.: Integrated lithospheric strength (Pa m) and strength variations (Pa) along two cross-sections estimated for a compressional regime using the crustal rheological types (Fig. 2) and (a) the NA07 thermal model (Fig. 1a); (b) the SL2013sv thermal model (Fig. 1b). Black circles as in Figs. 4(a-b) show the intraplate earthquakes location from the seismic catalog for stable continental regions (SRCs) of Schulte and Mooney (2005).

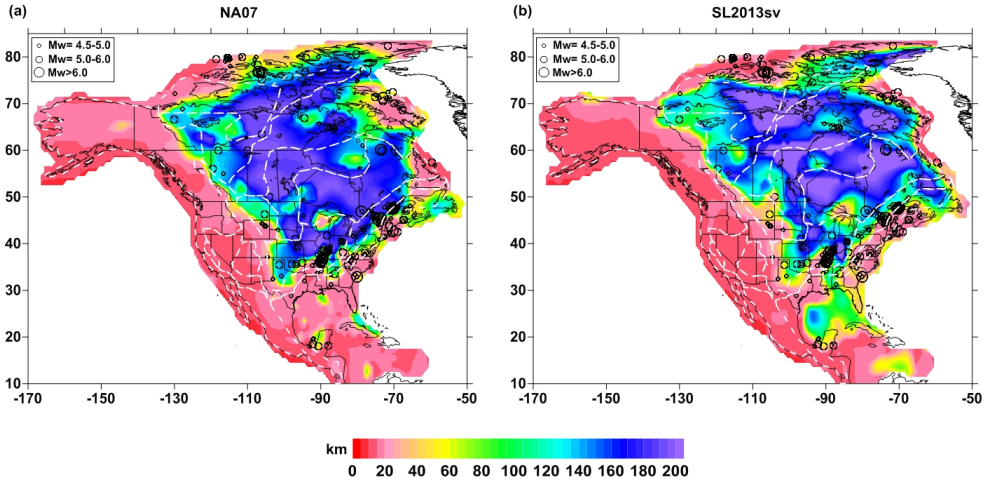

Fig. 4.: Effective elastic thickness (Te) of the lithosphere (km) (Tesauro et al., 2014a) for (a) NA07 and (b) SL2013sv.

Scientific Programme

GeoMod2014 - Conference Outline

Time	31. August	1. September	2. September	3. September
08:45 - 09:00	-	Welcome	-	-
09:00 - 11:00	-	(Seismo-)tectonics (orals)	Volcanism and Volcanotectonics (orals)	Rheology (orals)
11:00 - 13:00	-	(Seismo-)tectonics (posters)	Volcanism and Volcanotectonics (poster)	Rheology (poster)
13:00 - 14:00	-	Lunch break	Lunch break	Lunch break
14:00 - 16:00	-	Tectonics and Surface processes (orals)	Geodynamics (orals)	Fluids and Deformations (orals)
16:00 - 18:00	-	Tectonics and Surface processes (poster)	Geodynamics (posters)	Fluids and Deformations (poster)
18:00 - 21:00	Ice Breaker Party	-	-	-
19:00 - 22:00	-		Joint Conference Dinner	-

GeoMod2014 - Short course on "Constitutive Laws: from Observation to Implementation in Models" by Onno Oncken, Mathias Rosenau, Fabio Corbi, Georg Dresen Erik Rybacki, Stephan Sobolev, and Sascha Brune
Thursday 4 September: 09:00 - 18:00
Friday 5 September: 09:00 - 14:00

GeoMod2014 - Hands-on tutorial on "ASPECT: a next-generation geodynamic modelling software" by Anne Glerum and Juliane Dannberg
Thursday 4 September: 09:00 - 18:00: Tutorial
Friday 5 September: 09:00 - 18:00: ASPECT Strategy Workshop (for Advanced Users) - voluntary

GeoMod2014 Conference Programme (31 August - 3 September)

Sunday 31 August 2014

18:00 - 21:00: Ice Breaker Party at the 'Theaterschiff Potsdam' (Schiffbauergasse 9b, 14467 Potsdam)

Monday 1 September 2014

08:45 - 09:00: Welcome by Prof. Dr. Dr. h.c. Reinhard Hüttl and Prof. Dr. Onno Oncken

09:00 - 11:00: (Seismo-)tectonics Orals (chairs: B. Kaus, O. Oncken)

- 09:00 - 09:30: **Kelin Wang:** *Thermal Expressions of Stick-slip and Creeping Subduction Megathrusts* (keynote)
- 09:30 - 10:00: **Bertrand Maillot:** *The long-term Evolution of Fold-and-Thrust Belts: Consistency of Numerical Approaches and Physical Experiments* (keynote)
- 10:00 - 10:20: **Tasca Santimano** et al.: *Smart or Beautiful? Accretionary wedge evolution seen as a competition between minimum work and critical taper*
- 10:20 - 10:40: **Lorenzo Bonini** et al.: *The role of pre-existing frictional weaknesses on the propagation of extensional faults*
- 10:40 - 11:00: **Ylona van Dinther** et al.: *Seismo-thermo-mechanical modeling of subduction zone seismicity*

11:00 - 13:00: (Seismo-)tectonics Posters (chairs: B. Kaus, O. Oncken)

13:00 - 14:00: Lunch break

14:00 - 16:00: Tectonics and Surface processes Orals (chairs: F. Graveleau, N. Hovius)

- 14:00 - 14:30: **Ritske Huismans:** *Interaction and feedback between surface processes and mountain building* (keynote)
- 14:30 - 15:00: **Stéphane Dominguez:** *Joint analogue modelling of marine and terrestrial geological processes: state of the art and new developments* (keynote)
- 15:00 - 15:15: **Utsav Mannu** et al.: *Dynamic Modelling of Accretionary Prisms and Stratigraphy of Forearc basins*
- 15:15 - 15:30: **Karen Leever:** *3D Analogue Modelling of the Effect of Fan Sedimentation on Accretionary Wedge Dynamics – the Magdalena Fan case, South Caribbean Margin, Colombia*
- 15:30 - 15:45: **Frank Zwaan**, Guido Schreurs: *4D Transfer Zone Modeling in Continental Rift Systems*
- 15:45 - 16:00: **Sergei Medvedev**, Ebbe H. Hartz: *Evolution of topography of post-Devonian Scandinavia: Effects and rates of erosion*

16:00 - 18:00: Tectonics and Surface processes Posters (chairs: F. Graveleau, N. Hovius)

Tuesday 2 September 2014

09:00 - 11:00: Volcanism and Volcanotectonics Orals (chairs: O. Galland, E. Holohan)

- 09:00 - 09:30: **Rikke Pedersen:** *Surface deformation simulations of volcanic and tectonic processes in Iceland* (keynote)
- 09:30 - 10:00: **Olivier Roche**, Yarko Niño: *Mechanisms of entrainment of a granular substrate by pyroclastic density currents: insights from laboratory experiments and models, and implications for flow dynamics* (keynote)
- 10:00 - 10:15: **Rosanne Heistek** et al.: *Temporal changes in mantle wedge geometry and magma generation processes in the Central Andes: towards linking petrological data to thermomechanical models*
- 10:15 - 10:30: **Francesco Maccaferri** et al.: *The gravitational unloading due to rift depression: A mechanism for the formation of off-rift volcanoes in (continental) rift zones*
- 10:30 - 10:45: **Lola Chanceaux**, Thierry Menand: *Solidification effects on sill formation: an experimental approach*
- 10:45 - 11:00: Max Gallagher, **Ben Kennedy** et al.: *Megatsunami generation from caldera subsidence*

11:00 - 13:00: Volcanism and Volcanotectonics Posters (chairs: O. Galland, E. Holohan)

13:00 - 14:00: Lunch break

14:00 - 16:00: Geodynamics Orals (chairs: F. Funiciello, S. Sobolev)

- 14:00 - 14:30: **Anne Davaille:** *Plumes to Plate Tectonics: Insights from Laboratory Experiments* (keynote)
- 14:30 - 15:00: **Bernhard Steinberger** et al.: *On the relation between plate tectonics, large-scale mantle flow and mantle plumes: Some recent results and many open questions* (keynote)
- 15:00 - 15:15: **Paul J. Tackley** et al.: *Influence of Melting on the Long-Term Thermo-Chemical Evolution of Earth's Deep Mantle*
- 15:15 - 15:30: **Maria V. Chertova** et al.: *3-D numerical modeling of subduction evolution of the western Mediterranean region*
- 15:30 - 15:45: Tobias Baumann, **Boris Kaus**, A. Popov: *Constraining the rheology of the lithosphere through geodynamic inverse modelling*
- 15:45 - 16:00: **Elisa Calignano** et al.: *Strain localization during compression of a laterally heterogeneous lithosphere*

16:00 - 18:00: Geodynamics Posters (chairs: F. Funiciello, S. Sobolev), Methods and Materials Posters (chairs: M. Frehner, M. Rosenau)

19:00 - 22:00 Joint conference dinner in Potsdam on the ship 'Belvedere' (Lange Brücke 6, 14467 Potsdam)

Wednesday 3 September 2014

09:00 - 11:00: Rheology Orals (chairs: G. Dresen, H. Sone)

- 09:00 - 09:30: **Yuri Fialko:** *Numerical models of ductile roots of mature strike-slip faults* (keynote)
- 09:30 - 10:00: **Laurent Montési:** *Localization processes on Earth, Mars, and Venus* (keynote)
- 10:00 - 10:20: **Suzon Jammes** et al.: *Localization of deformation in a polymineralic material*
- 10:20 - 10:40: **Sebastian P. Müller** et al.: *Rheology of bubble- and crystal-bearing magma: new analogue experimental data and an effective-medium model*
- 10:40 - 11:00: **Maria A. Nikolinakou** et al.: *Modeling stress evolution around a rising salt diapir*

11:00 - 13:00: Rheology Posters (chairs: G. Dresen, H. Sone)

13:00 - 14:00: Lunch break

14:00 - 16:00: Fluids and Deformations Orals (chairs: S. Miller, M. Moreno)

- 14:00 - 14:30: **Boris Galvan** et al.: *Towards a general simulation tool for complex fluid-rock lithospheric processes: merging pre-processing, processing and post-processing in state-of-the-art computational devices* (keynote)
- 14:30 - 15:00: **Takeshi Tsuji:** *Digital rock physics: Insight into fluid flow and elastic deformation of porous media* (keynote)
- 15:00 - 15:15: **Thomas Heinze** et al.: *Numerical Modelling of earthquake swarms in the Vogtland / West- Bohemia*
- 15:15 - 15:30: **Samuel Angiboust** et al.: *Effect of Fluid Circulation on Intermediate-Depths Subduction Dynamics: From Field Observations to Numerical Modelling*
- 15:30 - 15:45: Magdalena Scheck-Wenderoth, **Judith Sippel** et al.: *Heat transport mechanisms at different scales – a 3D modelling workflow*
- 15:45 - 16:00: **Antoine Jacquey** et al.: *Modelling of fractured reservoirs: Fluid-rock interactions within fault domains*

16:00 - 18:00: Fluids and deformations Posters (chairs: S. Miller, M. Moreno)

The posters will be presented during the entire conference. Each poster session starts with a 1-2 min. short presentation of all participating posters.

GeoMod2014 - Short course on "Constitutive Laws: from Observation to Implementation in Models"

Thursday 4 September 2014

Morning Session: Onno Oncken, Mathias Rosenau, and Fabio Corbi

- 09:00 - 10:00: **Onno Oncken:** Observing deformation kinematics and localization: Observations from the field, geophysical imaging, and geodetic monitoring
- 10:00 - 10:15: Coffee Break
- 10:15 - 11:00: **Mathias Rosenau:** Rheology of rock analogues 1: Elastoplasticity and its application in seismotectonic simulation
- 11:00 - 11:15: Coffee Break
- 11:15 - 12:00: **Fabio Corbi:** Rheology of rock analogues 2: Viscoelasticity and its application in seismotectonic simulation
- 12:00 - 13:00: **Visit to the GFZ Analogue Lab**

13:00 - 14:00: Lunch break

Afternoon Session: Georg Dresen and Erik Rybackii

- 14:00 - 15:15: Rheology of the lower crust : Reconciling laboratory data and field observations
- 15:15 - 15:30: Coffee Break
- 15:30 - 16:45: **Visit to the GFZ rock mechanics lab**
- 16:45 - 17:00: Coffee Break
- 17:00 - 18:00: Rock fracture processes and stick slip sliding –What do we learn from analyzing nanofemto seismicity?

Friday 5 September 2014

Morning Session: Stephan Sobolev and Sascha Brune

- 09:00 - 10:00: **Stephan Sobolev:** Rheology and geodynamic modeling: key controls in plate tectonics and beyond
- 10:00 - 10:15: Coffee Break
- 10:15 - 11:30: **Sascha Brune:** Rock rheology in numerical models: PC exercises and application to rift dynamics
- 11:30 - 11:45 Coffee Break
- 11:45 - 12:30: **Stephan Sobolev:** Rheology and cross-scale modeling: towards understanding of great earthquakes
- 12:30 - 13:00: Discussion

13:00 - 14:00: Lunch and end of the short course

GeoMod2014 – Hands-on tutorial on"ASPECT: a next-generation geodynamic modelling software" by Anne Glerum and Juliane Dannberg

Thursday 4 September 2014

08:30 - 9:00: Registration

- 09:00 - 10:00: **Tutorial 1:** First Steps – Compiling and Running ASPECT, **Lecture:** How to run and visualize simple models
- 10:00 - 11:15: **Lecture** ASPECT – A next-generation geodynamic modelling software, **Tutorial 2:** Convection in a 2D box
- 11:15 - 11:30: Coffee Break
- 11:30 - 13:00: **Tutorial 3:** Using the adaptive mesh refinement and spherical shell geometry **Lecture:** How to run and visualize simple models

13:00 - 14:00: Lunch break

- 14:00 - 15:15: **Tutorial 4:** Using the adaptive mesh refinement and spherical shell geometry and using the function parser
- 15:15 - 15:30: Coffee Break
- 15:30 - 17:00: **Tutorial 5:** Averaging at the example of subduction and using a “sticky air” layer
- 17:00 - 18:00: **Voluntary:** Installing ASPECT on personal computers

18:30: Joint Dinner (to be payed by the participants)

Friday 5 September 2014

09:00 - 18:00: ASPECT Strategy Workshop for Advanced Users: Perspectives for Modelling with ASPECT

Index